Chapter 3

Convective Instability of Thickening Mantle Lithosphere

Abstract. Mantle lithosphere, being colder and therefore denser than the underlying mantle, is prone to convective instability that can be induced by horizontal shortening. Numerical experiments on a cold layer with imposed horizontal shortening were carried out to examine the relative importance of mechanical thickening, thermal diffusion, and gravitational instability in deforming the layer. This analysis is then used to develop a method for determining which of these styles dominates for a layer thickening at a given rate. If viscosity is non-Newtonian, the imposition of shortening decreases the lithospheric strength, which causes perturbations to the lithosphere's temperature structure to grow exponentially with time. Once these perturbations become sufficiently large, they then grow super-exponentially with time, eventually removing the lithospheric base. Because lithospheric viscosity is highly temperature-dependent, at most only the lower 30% of the lithosphere participates in the downwelling associated with this initial super-exponential growth event. After this event, however, a downwelling develops that removes material advected into the region of downwelling by horizontal shortening. The magnitude of this persistent downwelling depends on the rate and duration of shortening. If the total amount of shortening does not exceed 50% (doubling of crustal thickness), then this downwelling extends to a depth 3 to 4 times the thickness of undeformed lithosphere and forms a

sheet significantly thinner than the width of the region undergoing shortening. Once shortening stops, this downwelling is no longer replenished by the shortening process, and should then detach due to its inherent gravitational instability. The hottest 60% of the mantle portion of the lithosphere could be removed in such an event, which would be followed by an influx of hot, buoyant asthenosphere that causes rapid surface uplift. Because more cold material is removed after the cessation of shortening than by the initial gravitational instability, the former has a potentially greater influence on the amount of surface uplift. The Tibetan interior is thought to have been shortened by about 50% in ~ 30 million years and afterward, at approximately 8 Ma, experienced a period of rapid uplift that may have resulted from the removal of a large downwelling "finger" of cold lithosphere generated by shortening.

3.1 Introduction

Thickening of the crust is one consequence of horizontal convergence at the Earth's surface and is the main process by which mountains are built. Thickening of mantle lithosphere may occur as well, and has been proposed as an accompanying process that may also affect mountain building. In particular, thickening should enhance the gravitational instability of cold, dense mantle lithosphere with respect to the hot, buoyant asthenosphere beneath it (Figure 3.1a) [e.g., *Fleitout and Froidevaux,* 1982; *Houseman, McKenzie and Molnar,* 1981]. If the mantle lithosphere becomes sufficiently unstable, localized convective downwelling, of the type described by *Howard* [1964], may be initiated at the base of the mantle lithosphere (Figure 3.1b). The subsequent removal of cold lithosphere, and its replacement by hot mantle, could result in rapid surface uplift followed by extension [e.g., *Bird,* 1979; *England and Houseman,* 1989; *Neil and Houseman,* 1999]. This process is thought to have caused rapid uplift of the Tibetan plateau 8 million years ago [*Harrison et al,* 1992; *Molnar, England, and Martinod,* 1993], and has been inferred for other mountain belts [*Houseman and Molnar,* 1997; *Platt and England,* 1994; *Platt et al.,* 1998].

The gravitational instability of mantle lithosphere can be enhanced by thickening

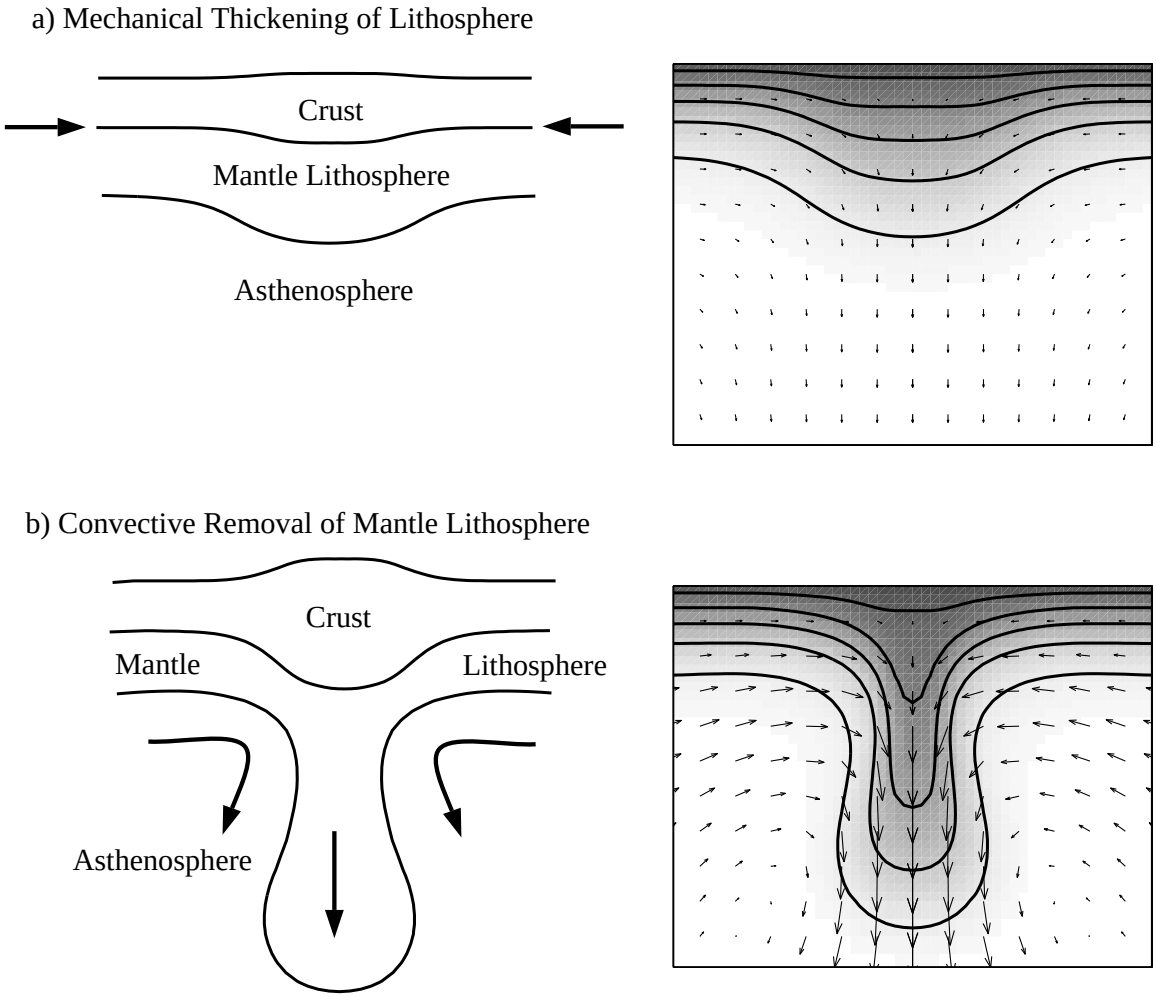

Figure 3.1: Cartoons showing (a) horizontal shortening and thickening of the lithosphere, which includes both the crustal layer and the lithosphere's mantle portion. Mechanical thickening should enhance the gravitational instability of the cold, dense, mantle lithosphere with respect to the hot asthenosphere below. If the mantle lithosphere is made sufficiently unstable, its lower portion may be removed in a localized convective downwelling, drawn in (b). Removal of mantle lithosphere and its replacement by hot asthenosphere could result in rapid uplift at the surface. Shown on the right in both (a) and (b) is output from a numerical experiment that shows the generation of convective instability by mechanical thickening of a cold, dense layer. Here arrows represent velocity and show horizontal shortening of the central region in (a) and a faster flow associated with convective downwelling in (b). Temperature, represented by shades of gray (colder is darker) and contours (evenly spaced temperature intervals), clearly shows the removal of the cold layer's basal portion.

in several ways. First, thickening increases the amount of dense, potentially unstable material in a thickened region [e.g., *Conrad and Molnar,* 1999; *Fleitout and Froidevaux,* 1982; *Houseman, McKenzie and Molnar,* 1981]. Second, if lithospheric rocks deform by a nonlinear stress-strain relationship, as they are observed to do in laboratory experiments, the strain-rates associated with shortening should decrease the background strength of the lithosphere and enhance its gravitational instability [*Molnar, Houseman, and Conrad,* 1998]. Finally, nonuniform thickening generates large variations in the lithosphere's stratified temperature field, allowing gravitational instability to grow from accompanying variations in the density field. If viscosity is non-Newtonian, the strain-rates associated with the growing instability decrease the lithosphere's strength and cause the instability to grow more rapidly. This process accelerates into a rapid removal of the lithospheric base [e.g., *Canright and Morris,* 1998; *Conrad and Molnar,* 1999; *Houseman and Molnar,* 1997].

These mechanisms of promoting gravitational instability of the lithosphere have been studied by approximating the convective instability as a Rayleigh-Taylor instability, in which diffusion of heat is ignored. Thermal diffusion, however, smooths perturbations to the lithosphere's stratified temperature field, and thus may retard, or even prevent, their growth as part of convective instability. *Conrad and Molnar* [1999] address this issue by including the stabilizing effects of thermal diffusion for a generalized density and viscosity structure. These authors, however, study instability only in layers that are already convectively unstable, and consider horizontal shortening only as a mechanism that allows the lithosphere to thicken into an unstable state. The role of horizontal shortening in making lithosphere unstable is treated more fully by *Molnar, Houseman and Conrad* [1998], but their studies do not include thermal diffusion. Thus, an analysis of the full convective instability for a layer that is undergoing horizontal shortening is needed.

The numerical experiments described below, which are similar to those exemplified in Figure 3.1, simulate mantle lithosphere that eventually becomes convectively unstable because it thickens. I compare the deformation that results to the unstable growth predicted by simpler studies of the Rayleigh-Taylor instability for different

rheologies [e.g., *Conrad and Molnar,* 1997; 1999; *Houseman and Molnar,* 1997], undergoing horizontal shortening [e.g., *Molnar, Houseman, and Conrad,* 1998], and in conjunction with thermal diffusion [e.g., *Conrad and Molnar,* 1999]. The rheological conditions and magnitudes of shortening rates that generate the various types of gravitational instability can then be determined in a general way through the use a dimensionless scaling analysis, as can the approximate time-dependent behavior of a growing instability. Finally, I attempt to determine how much material may be removed by convective instability in a thickening environment, and the effect of this removal on the remaining lithosphere. As a result, this study treats the full convective instability of thickening mantle lithosphere more completely than do previous analyses. Because they build upon previously-developed scaling analyses for various aspects of the the full problem treated here, these results are comprehensive, but easily applied to gravitationally unstable layered structures such as the mantle lithosphere.

3.2 Review of Rates for Unstable Growth

The convective stability of a thickening cold thermal boundary layer can be studied by observing the behavior of small perturbations to the boundary layer's stratified temperature field. Various time scales are associated with different mechanisms that promote the growth or decay of these perturbations. The first growth mechanism is the shortening process itself, which advects cold material downward as the layer thickens, and therefore amplifies perturbations to the temperature field [e.g., *Bassi and Bonnin,* 1988; *Fletcher and Hallet,* 1983; *Ricard and Froidevaux,* 1986; *Zuber, Parmentier, and Fletcher,* 1986]. Two types of growth are associated with the gravitational instability of a dense fluid overlying a less dense fluid, also known as a Rayleigh-Taylor instability. If the viscosity of the deforming fluid is independent of strain-rate, perturbations initially grow exponentially with time [e.g., *Chandrasekhar,* 1961; *Conrad and Molnar,* 1997; *Whitehead and Luther,* 1975]. For non-Newtonian viscosity, growth is super-exponential with time [e.g., *Canright and Morris,* 1993; *Houseman and Mol-*

nar, 1997]. Finally, the lithosphere's density field is perturbed through temperature, which is subject to thermal diffusion. Thermal diffusion smooths temperature variations, and thus diminishes the amplitude of density perturbations, slowing, or even preventing, their unstable growth [e.g., *Rayleigh,* 1916].

The complete convective instability of a thickening boundary layer with non-Newtonian viscosity can thus be ideally described as the simultaneous action of (a) mechanical thickening, (b) exponential followed by (c) super-exponential growth of perturbations, and (d) thermal diffusion acting to suppress growth. Each mechanism operates with a characteristic timescale that depends on size of the perturbation itself and on the physical properties of the layer. In general, one of the four mechanisms has a dominant influence on the behavior of perturbations because it induces growth or decay of perturbations at significantly faster rates than do the others. In what follows, expressions for these growth or decay rates are developed. These expressions are later used to construct dimensionless parameters that compare the relative importance of the different mechanisms in deforming a given thermal boundary layer that is undergoing horizontal shortening.

3.2.1 Exponential Growth

If thermal diffusion is ignored, perturbations to an unstable density structure grow in a manner that can be described by an analysis of the Rayleigh-Taylor instability. In this analysis, it is useful to describe deformation of a fluid by a strain rate, $\dot{\epsilon}_{ij}$, defined in terms of the components of velocity, u_i:

$$\dot{\epsilon}_{ij} = \frac{1}{2}\left(\frac{\partial u_i}{\partial x_j} + \frac{\partial u_j}{\partial x_i}\right) \tag{3.1}$$

The flow field is incompressible, meaning that $\dot{\epsilon}_{ii} = 0$. In a highly viscous fluid, gravitational body forces are balanced by viscous stresses associated with flow. This flow, described by the strain rate, is related to the deviatoric stress, τ_{ij}, by:

$$\tau_{ij} = 2\eta\dot{\epsilon}_{ij} \tag{3.2}$$

The effective viscosity, η, can vary with temperature and may depend on strain rate:

$$\eta = \frac{B}{2}\dot{E}^{\left(\frac{1}{n}-1\right)} \tag{3.3}$$

where B is a rheological parameter, n is a power law exponent, and $\dot{E}^2 = (1/2)\sum_{i,j}\dot{\epsilon}_{ij}\cdot\dot{\epsilon}_{ij}$ is the second invariant of the strain-rate tensor. Dislocation creep of olivine in the lithosphere is often described using (3.3) and n about 3.5 [e.g., *Kohlstedt, Evans, and Mackwell,* 1995].

For Newtonian viscosity ($n = 1$), $\eta = B/2$ is a constant. In this case, perturbations to an unstable density structure grow exponentially with time [e.g., *Chandrasekhar,* 1961; *Conrad and Molnar,* 1997]. Thus, if Z is the magnitude of a sinusoidal perturbation of wavelength λ, and $w = dZ/dt$ is its downward speed, both obey:

$$\frac{dw}{dt} = qw \qquad \text{and} \qquad \frac{dZ}{dt} = qZ \tag{3.4}$$

where q is the exponential growth rate.

Conrad and Molnar [1999] nondimensionalize time and length according to:

$$t' = t\frac{\rho g \alpha T_0 h}{2\eta_m}F_1 \qquad \text{and} \qquad z' = \frac{z}{h} \tag{3.5}$$

where ρ is the mantle density, α is the thermal expansivity, g is the gravitational acceleration, T_0 is the temperature difference across the layer, h is the thickness of the unstable layer, and η_m is the Newtonian viscosity at the base of the layer. The parameter F_1 is a constant that accounts for the temperature dependence of viscosity, termed the "available buoyancy" by *Conrad and Molnar* [1999], who show that F_1 is given by the integral through the layer of the thermal buoyancy divided by the viscosity. Because colder portions of the layer are also stronger, the "available buoyancy" scaling quantifies the portion of the total buoyancy that is sufficiently weak to participate in the gravitational downwelling. Thus, the scaling of time given by (3.5) applies for cold layers with Newtonian viscosity, and arbitrary dependence of viscosity on temperature.

Using (3.5) to nondimensionalize (3.4) yields an expression for a dimensionless growth rate q', which can be related to the dimensional growth rate, q, according to:

$$q = \frac{\rho g \alpha T_0 h}{2\eta_m} F_1 q' \tag{3.6}$$

Using numerical experiments, *Conrad and Molnar* [1999] measure a maximum value of $q' \sim 0.2$ for dimensionless wavelengths close to $\lambda' = \lambda/h = 4$. The combination of (3.4) and (3.6) provides an estimate of the downward speed at the bottom of a perturbation growing exponentially with time:

$$w_1 = \frac{dZ}{dt} = \frac{\rho g \alpha T_0 h}{2\eta_m} F_1 q' Z \tag{3.7}$$

where the subscript of w_1 refers to the value of the power-law exponent, $n = 1$.

If viscosity is non-Newtonian ($n > 1$), η_m decreases as strain-rates increase, as shown by (3.3). For a dense layer undergoing horizontal shortening, strain-rates are associated with both horizontal shortening and unstably growing perturbations. For sufficiently small perturbation amplitudes, the strain-rates due to shortening are greater, and thus determine the effective viscosity of the dense layer. As long as this viscosity remains constant, perturbations grow exponentially with time and with growth rate given by (3.6), where the viscosity is given by (3.3). Once strain-rates associated with the growing perturbation begin to dominate those due to shortening, effective viscosity is affected and growth proceeds super-exponentially, as described below. Thus, as suggested by *Conrad and Molnar* [1997] and confirmed by *Molnar, Houseman and Conrad* [1998], perturbations may grow exponentially with time even if viscosity is non-Newtonian, but only if their amplitude is sufficiently small.

3.2.2 Super-Exponential Growth

An increase in the amplitude of a growing perturbation causes an increase in strain-rates, and thus a decrease in the effective viscosity of a non-Newtonian fluid ($n > 1$). This decrease in viscosity causes a density instability to grow super-exponentially with

time [e.g., *Canright and Morris*, 1993; *Houseman and Molnar*, 1997]. By approximating $\dot{E} \sim w/h$, *Houseman and Molnar* [1997] obtain an expression for the time-varying viscosity using (3.3). This leads to an expression for the downward speed, w_n, of:

$$w_n = \frac{dZ}{dt} = \left(\frac{C}{n}\right)^n \left(\frac{\rho_m g \alpha T_0}{B_m}\right)^n h F_n Z^n \tag{3.8}$$

where F_n is the "available buoyancy," which depends on n and the depth dependence of B, B_m is the value of B at the base of the unstable layer, and C is a dimensionless measure of the rate of growth [*Conrad and Molnar*, 1999]. Notice that when $n = 1$, (3.8) reduces to (3.7) and C is equivalent to q'. For $n = 3$, measurements of C for different dependences of B on T differ from 0.45 by about 20% [*Conrad and Molnar*, 1999].

Following *Houseman and Molnar* [1997], *Conrad and Molnar* [1999] suggest nondimensionalizing distance and time according to:

$$t'' = t\left(\frac{\rho g \alpha T_0 h}{B_m}\right)^n F_n \qquad \text{and} \qquad z'' = z' = \frac{z}{h} \tag{3.9}$$

where double primes indicate a nondimensionalization of time for super-exponential growth. Solving for w_n'' in terms of t'' yields:

$$w_n'' = \left[C\left(\frac{n-1}{n}\right)(t_b'' - t'')\right]^{\left(\frac{n}{1-n}\right)} \tag{3.10}$$

which indicates super-exponential growth [*Houseman and Molnar*, 1997]. Here t_b'' is the dimensionless time at which speed becomes infinite and the instability must be detached from the dense layer. By integrating (3.10), *Houseman and Molnar* [1997] show:

$$t_b'' = \left(\frac{n}{C}\right)^n \frac{Z_0'^{(1-n)}}{(n-1)} \tag{3.11}$$

where Z_0' is perturbation's initial amplitude.

3.2.3 Horizontal Shortening

Horizontal shortening of a layer generates thickening and causes the base of the layer to descend with a speed $w_s = dh/dt$. Incompressibility requires $\dot{\epsilon}_{xx} = -\dot{\epsilon}_{zz} = w_s/h$, giving:

$$w_s = \frac{dh}{dt} = \dot{\epsilon}_{xx} h \qquad \text{and} \qquad \frac{dw_s}{dt} = \dot{\epsilon}_{xx} w_s \tag{3.12}$$

A comparison to (3.4) shows that (3.12) is an expression for exponential growth. In this case, however, it is not the perturbation amplitude Z that grows exponentially with time, but the thickness of the entire layer h. The "growth rate" in this case is simply $\dot{\epsilon}_{xx}$.

3.2.4 Diffusion of Heat

The cooling of a boundary layer generates the negative buoyancy that drives convective instability. Conductive cooling of a halfspace, appropriate for the cooling of oceanic lithosphere, yields a temperature profile given by an error function:

$$T(z) = T_s + T_0 \, \mathrm{erf}(-z/h) \qquad \text{where} \qquad h = 2\sqrt{\kappa t_c} \tag{3.13}$$

Here t_c is the time during which the halfspace has cooled [e.g., *Turcotte and Schubert,* 1982, pp. 163-167] and T_s is the surface temperature. The rate at which an isotherm at depth h descends can be easily determined by taking the time derivative of h:

$$w_{d,v} = \frac{dh}{dt} = \sqrt{\frac{\kappa}{t_c}} = \frac{2\kappa}{h} \tag{3.14}$$

where the subscripts d and v denote diffusion in the vertical direction.

Diffusion of heat also smooths, and thus diminishes, the horizontal perturbations in temperature from which instability must grow [e.g., *Conrad and Molnar*, 1997; 1999]. Consider perturbations to the background temperature field of the form $\Delta T \sim \cos(kx)$, where ΔT is the temperature perturbation, $k = 2\pi/\lambda$ is the wavenumber, and x is horizontal distance. The horizontal temperature field is subject to the heat

conduction equation:

$$\frac{\partial \Delta T}{\partial t} = \kappa \left(\frac{\partial^2 \Delta T}{\partial x^2} \right) \tag{3.15}$$

where κ the the thermal diffusivity [e.g., *Turcotte and Schubert,* 1982, p. 154]. Perturbations decay exponentially with time as:

$$\frac{\partial \Delta T}{\partial t} = -\kappa \frac{4\pi^2}{\lambda^2} \Delta T \tag{3.16}$$

The wavelength, λ, should scale with the thickness of the layer, h. In addition, the amplitude of a perturbation to an isotherm, Z, should be linearly related to the amplitude of horizontal temperature variations, ΔT. Ignoring constants, horizontal thermal diffusion then generates a characteristic rate of:

$$w_{d,h} = \frac{dZ}{dt} \sim -\frac{\kappa Z}{h^2} \tag{3.17}$$

where the negative sign indicates a diminishment of perturbation amplitudes with time.

3.3 Numerical Experiments

Numerical experiments, similar to those performed by *Conrad and Molnar* [1999], can be used to search for the conditions under which each mode of deformation is dominant. I use the finite element code ConMan, which can solve the coupled thermal diffusion and incompressible Navier-Stokes equations for high Prandtl number [*King, Raefsky and Hager,* 1990]. Convective instability is initiated by imposing a temperature field as in (3.13). With an assigned thermal expansivity α, colder fluid is denser and flows downward into the underlying warm fluid as the instability grows. Perturbing (3.13) by applying:

$$h(x) \;=\; 2\sqrt{\kappa t_c}\sqrt{1 + p\cos(2\pi x/\lambda)} \tag{3.18}$$

where p is a constant that specifies the perturbation amplitude, initiates unstable growth. This corresponds to a sinusoidal variation in t_c, which imposes a smooth perturbation.

The finite element grid has a depth $8.27h$ and a width of $\lambda'/2 = 2.07h$. Perturbations with this wavelength grow most rapidly [*Conrad and Molnar*, 1999], and thus should reflect the unstable growth that occurs in a system initially perturbed at all wavelengths. The grid consists of 54 elements in the vertical direction, with 36 elements in the upper half of the box, giving double resolution in the region where the most of the deformation occurs. Eighteen elements in the horizontal direction make each element in the upper half of the box square. This resolution is coarser than that used by *Conrad and Molnar* [1999], but tests show that measurements of growth rate are only changed by a few percent.

Horizontal shortening is generated by imposing horizontal velocity boundary conditions along the vertical and top surfaces of the box. Specifically, the left side of the box has zero horizontal velocity, and a horizontal velocity of $-v$ is imposed along the right boundary. On both sides, free slip in the vertical direction is permitted. Along the top surface, the imposed velocity is zero in the vertical direction, and has a horizontal component that tapers linearly from zero on the left to $-v$ on the right. These boundary conditions set up a flow that allows the dense surface layer to thicken according to (3.12), where $\dot{\epsilon}_{xx} = 2v/\lambda$. Horizontal shortening could also have been implemented by imposing forces, instead of velocities, on the sides of the box. Although this method more closely resembles lithospheric shortening, which probably involves external forces acting on strong surface plates, it does not specify the location or the rate of thickening, making the resulting deformation more difficult to analyze. In this work, the pattern of shortening is imposed by the velocity boundary conditions, and an assumption is made that external forces could generate this pattern if present. Finally, no stress boundary conditions are imposed along the bottom boundary so that material is not constrained to circulate within the box, which could impede the flow. The box is sufficiently deep, however, that the sinking boundary layer accelerates to a terminal velocity before approaching the bottom of the box.

The imposition of zero vertical velocity at the surface ignores any downward deflection of the crust-mantle boundary, which may influence gravitational instability of the mantle lithosphere. For example, downward motion of the Moho is gravitationally unfavorable, which causes unstable growth below the Moho to be slowed by any Moho deflection that it creates [*Houseman et al.*, 1999; *Neil and Houseman*, 1999]. This effect, however, requires a coupling between deflection of the Moho and convective instability, and thus should be diminished if the cold lithosphere near the Moho is stronger than the downwelling portion of the mantle lithosphere. As a result, the stabilizing effects of a crustal layer should be negligible if viscosity is strongly temperature-dependent, as is considered here. On the other hand, Moho deflection induced by thickening should increase the rate at which the cold mantle lithosphere is forced downwards into the hot asthenosphere. This should increase the amplitude of perturbations, which, for non-Newtonian viscosity, increases the downward speeds associated with gravitational instability, as shown by (3.8). Thus, deflection of the Moho by horizontal shortening may promote convective instability.

Viscosity in this analysis is non-Newtonian, as described by (3.3), with a power-law exponent of $n = 3$. Following *Conrad and Molnar* [1999], B varies with temperature according to:

$$B(T) = B_m \exp(\ln(r)\frac{T_m - T}{T_0}) \tag{3.19}$$

where the parameter r is the total variation in B across the fluid's temperature range, and T_m is the temperature of the underlying fluid. Thus, $B(T_m) = B_m$ and $B(T_s = T_m - T_0) = rB_m$. The temperature dependence of viscosity is altered by varying r.

3.4 A Comparison of Rates for Unstable Growth

A dense layer of non-Newtonian fluid that is undergoing horizontal shortening should exhibit time-dependent growth or decay of perturbations that can be described predominantly by one of the above-mentioned modes of deformation. These modes include exponential and super-exponential growth of perturbations, uniform thickening

of the layer, and diffusion of heat in the vertical and horizontal directions. Equations (3.7), (3.8), (3.12), (3.14), and (3.17) provide expressions for w_1, w_3, w_s, $w_{d,v}$, and $w_{d,h}$, which are the downward speeds of isotherms near the bottom of an unstable temperature structure for each of these modes operating independently. In general, the dominant mode should be the one that causes the isotherms of a layer to move most rapidly. Because the above speeds depend on the material properties of the layer, the shortening rate, and the amplitude of the perturbations to the layer's temperature structure, the dominant mode should also depend on these quantities, and may change with time as perturbations grow.

In what follows, a series of numerical experiments is used to determine the dominant mode of deformation for various combinations of the relevant parameters. To apply these experiments generally, dimensionless numbers are constructed by taking ratios of various combinations of the expressions for speed given above. The numerically-determined set of parameter values for which a given mechanism deforms isotherms most rapidly can then be expressed as ranges of these dimensionless numbers. Thus, each deformation mechanism is dominating in its own region of dimensionless parameter space, and the boundaries between these regions define "critical" values of the dimensionless parameters. To determine the dominant mode of deformation for any given layer that is undergoing shortening, one needs only to estimate values for the dimensionless numbers defined below, and then compare these values to the measured "critical" values. A summary of the various dimensionless parameters and their critical values is given in Table 3.1.

3.4.1 Convective Instability: Unstable Growth and Thermal Diffusion

By studying a layer that is not undergoing horizontal shortening, *Conrad and Molnar* [1999] determine the basic requirements for convective instability. Their analysis recognizes that horizontal thermal diffusion causes perturbations to an unstable temperature structure to decrease in amplitude with speed $w_{d,h}$ given by (3.17). If

viscosity is effectively Newtonian ($n = 1$), exponential growth causes fluid to move downward with speed w_1 given by (3.7). The ratio of these two speeds yields a dimensionless number that is proportional to a "Rayleigh" number, analogous to the Rayleigh number commonly used in thermal convection, and measures the convective instability of a thermal boundary layer:

$$Ra_1 = \frac{\rho_m g \alpha T_0 h^3}{2\kappa\eta_m} F_1 \sim \frac{w_1}{w_{d,h}} \tag{3.20}$$

where the constant q' is ignored in the definition of Ra_1. If viscosity is non-Newtonian with power law exponent n, the downward speed is given by w_n in (3.8). In this case, the relevant dimensionless "Rayleigh" number becomes:

$$Ra_n = \left(\frac{\rho_m g \alpha T_0}{n B_m}\right)^n \frac{h^3 Z^{n-1}}{\kappa} F_n \sim \frac{w_n}{w_{d,h}} \tag{3.21}$$

Note that if $n = 1$, Ra_n becomes Ra_1.

Whether perturbations grow unstably or are damped by thermal diffusion depends on the relative values of w_n and $w_{d,h}$, and thus on the parameter Ra_n. A large value of Ra_n means that $w_n >> w_{d,h}$, and unstable growth should dominate. To determine the "critical" value of Ra_n above which a cold boundary layer becomes convectively unstable, *Conrad and Molnar* [1999] measure the downward speed of material with a temperature of $T' = T/T_0 = 0.9$ (near the base of the layer) as a function of time in a series of numerical experiments similar to those described above, but using $\dot{\epsilon}_{xx} = 0$. For $n = 1$, the initial slope of a plot of $\ln w'$ versus t', made dimensionless using (3.5), gives the dimensionless exponential growth rate, q'. Similarly, if $n > 1$, a plot of $w''^{-2/3}$ versus t'', where time is nondimensionalized according to (3.9), should have a slope of $-C(n-1)/n$, as shown by (3.10). Varying the viscosity η_m, or the viscosity coefficient B_m if $n > 1$, allows the growth rates q' or C to be determined as a function of Ra_1 or Ra_n.

Numerical experiments [*Conrad and Molnar*, 1999] show that for large Ra_1, growth occurs with dimensionless growth rates close to $q' \sim 0.2$. If, however, $Ra_1 < 1000$, measured values of q' are less than 0.2, and for $Ra_1 < 100$ they become negative.

Negative values of q' indicate that perturbation amplitudes are diminished by the diffusion of heat faster than they can grow. Results are similar for $n = 3$, where $C \sim 0.45$ for $Ra_3 > 1000$ and negative for $Ra_1 < 100$. Thus, the "critical" value of Ra_n is about 100, at least for $n = 1$ and $n = 3$. If $Ra_n > 100$, unstable growth occurs; otherwise, the layer is stable to convection.

3.4.2 Horizontal Shortening and Thermal Diffusion

Now consider a layer of fluid with non-Newtonian viscosity and large B such that $Ra_3 < 100$, and that thickens due to an imposed horizontal strain-rate $\dot{\epsilon}_{xx}$. As described above and by *Conrad and Molnar* [1999], such a layer should be convectively stable, so that any heat transfer must be due either to advection by the imposed horizontal shortening or to thermal diffusion. Horizontal shortening causes the bottom of a layer to descend with velocity w_s, as shown by (3.12). Isotherms also grow deeper due to cooling from above, at a rate given by (3.14) as $w_{d,v}$. The ratio of these two rates yields a dimensionless quantity defined here as P because it is similar to a Peclet number, which compares rates of advective and diffusive heat transport:

$$P = \frac{\dot{\epsilon}_{xx} h^2}{\kappa} \sim \frac{w_s}{w_{d,v}} \tag{3.22}$$

where the factor of 2 is omitted for simplicity. If P is large, boundary layers thicken due to horizontal shortening, but if P is small, they thicken by cooling.

The "critical" value of P for which the transition between these two types of thickening occurs is determined by first measuring the downward velocity, w, of the $T' = 0.9$ isotherm as a function of time for many different values of P. Thickening of the layer by horizontal shortening alone causes dimensionless velocity and time to be related according to:

$$\frac{w'''}{w'''(t''' = 0)} = \exp t''' \qquad \text{where} \qquad t''' = t\dot{\epsilon}_{xx} \tag{3.23}$$

which is obtained by nondimensionalizing the expression for dw_s/dt in (3.12) and

integrating. According to (3.23), a plot of $\ln(w''')$ versus t''' should have a slope of unity if shortening is dominant. The measured value of this slope is a "growth rate" that is nondimensionalized by $\dot{\epsilon}_{xx}$ and termed q''' here. It is clear from Figure 3.2 that $q''' \sim 1$ for P greater than about 10, which is consistent with uniform thickening. Because these measurements are for a layer that is convectively stable ($Ra_n < 100$), thickening alone must dominate for $P > 10$.

For P less than about 1, q''' increases with decreasing P (Figure 3.2), which indicates that growth occurs more rapidly than would be expected for a layer experiencing only mechanical thickening. This is because, for sufficiently small P, horizontal shortening is slow enough that isotherms move downward more rapidly due to cooling than they do because of thickening. Because the velocity of the *fluid* at the location of a given isotherm is measured and not the vertical motion of of the isotherm itself, the measurement of w''' is still that of the thickening layer, given by (3.12), where h is the depth of the given isotherm. This velocity measurement increases with time, however, because isotherms move downward due to cooling according to (3.14), causing w''' to be measured at increasingly larger values of h. In short, cooling causes the sampling point (a given isotherm) to move to deeper locations within the fluid, locations where the fluid velocity given by (3.12) is greater. The measured value of the downward speed thus changes with time according to:

$$\frac{dw}{dt} = \frac{\partial w}{\partial h}\frac{\partial h}{\partial t} = \dot{\epsilon}_{xx}\frac{2\kappa}{h} = \frac{2\kappa}{h^2}w \tag{3.24}$$

where (3.12) gives $\partial w/\partial h$ and (3.14) gives $\partial h/\partial t$. By analogy to (3.4), (3.24) is an expression for exponential growth with growth rate $q = 2\kappa/h^2$. When made dimensionless using $\dot{\epsilon}_{xx}$, this growth rate can be simplified to $q''' = 2/P$. This relation approximates the measured values of q'''_s for $P < 1$ (Figure 3.2), meaning that vertical thermal diffusion dominates in this range.

At small values of P, measured growth rates become negative (Figure 3.2). This occurs because the layer is convectively stable ($Ra_1 < 100$ and $Ra_3 < 100$), so that horizontal thermal diffusion causes perturbation amplitudes to decrease with time. If

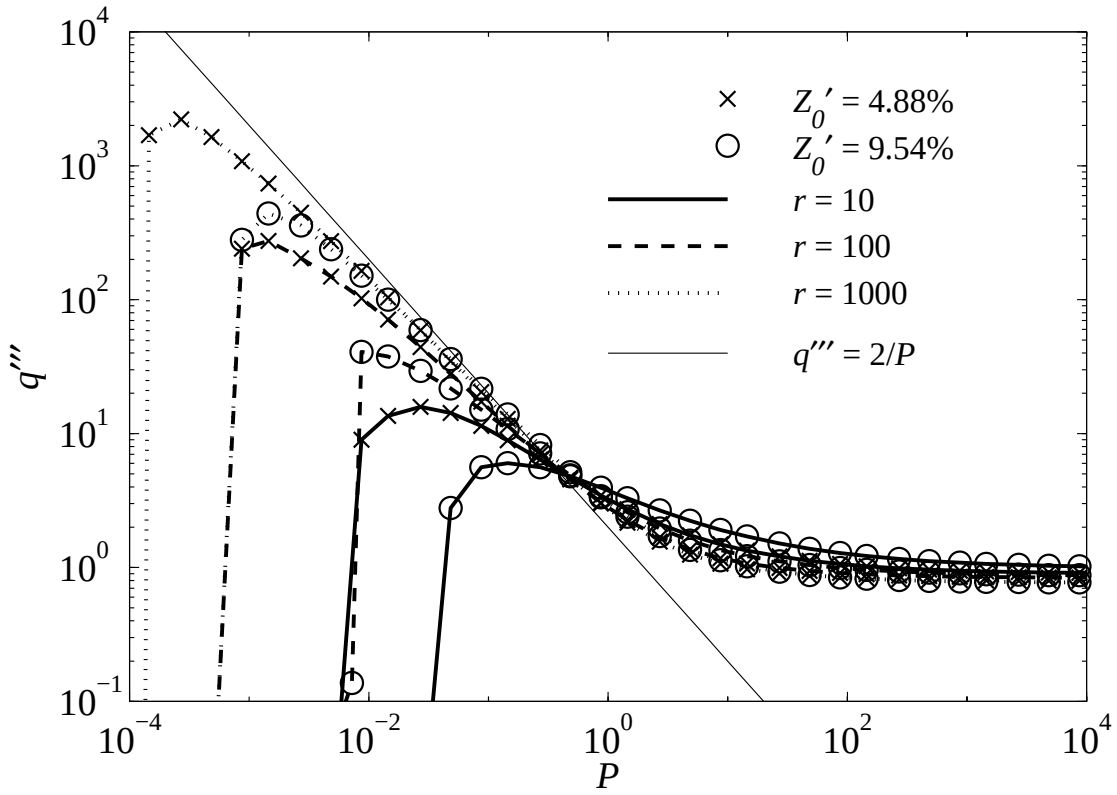

Figure 3.2: Plot of the initial dimensionless "growth rate," $q''' = q/\dot{\epsilon}_{xx}$, as a function of P, which is varied by varying $\dot{\epsilon}_{xx}$. Here q''' is determined by measuring the initial slope of a plot of $\ln(w_s''')$ versus t''', where time is made dimensionless using $t''' = t\dot{\epsilon}_{xx}$. Theory predicts that $q''' \sim 1$ if the depth of isotherms increases solely because of horizontal shortening, which is observed for $P > 10$. If isotherms deepen due to cooling from above, theory predicts $q''' \sim 2/P$, which is observed for $P < 1$ (thin solid line). At sufficiently small P, $q''' < 0$ because horizontal thermal diffusion causes perturbations to decrease in amplitude faster than shortening thickens the layer. Growth rates are calculated as described in the text for a set of parameters that yield $Ra_3 = 26000 Z_0'^2 F_3$. The maximum value of Ra_3 is then 0.7 for $Z_0' = 9.54\%$ and $r = 10$. The maximum value of Ra_1 is 0.7 for this same curve at $P \sim 10^4$. Thus, measured growth rates should only be affected by horizontal shortening and thermal diffusion because both Ra_1 and Ra_3 are below their critical values for convective instability.

horizontal strain-rates, expressed by P, are sufficiently small, this leads to negative measurements of the growth rate, as *Conrad and Molnar* [1999] found for convective instability.

3.4.3 Convective Instability and Horizontal Shortening

A layer undergoing horizontal shortening may also deform due to gravitational instability. If $Ra_3 > 100$, perturbations grow super-exponentially with time, at least after the effective viscosity is governed by strain-rates associated with the growing instability. If background strain-rates are larger than those induced by the instability, however, horizontal shortening induces a background Newtonian viscosity given by (3.3) that should promote initially exponential growth [*Molnar, Houseman and Conrad*, 1998]. For still larger imposed strain-rates, uniform thickening may overwhelm either the exponential or super-exponential growth associated with gravitational instability.

A transition from super-exponential to exponential growth of perturbations is thus expected at some imposed background strain-rate. The downward speed of a perturbation growing super-exponentially is given by (3.8) if $n = 3$ and should be independent of $\dot{\epsilon}_{xx}$. The downward speed associated with exponential growth is given by (3.7) and increases with $\dot{\epsilon}_{xx}^{2/3}$ because the effective viscosity given by (3.3) for $n = 3$ is proportional to $\dot{\epsilon}_{xx}^{-2/3}$. The ratio of these two speeds is proportional to the ratio Ra_1/Ra_3 and is given by:

$$\frac{Ra_1}{Ra_3} = 3\left(\frac{3B}{\rho g \alpha T_0 Z}\right)^2 \frac{F_1}{F_3}\dot{\epsilon}_{xx}^{2/3} \sim \frac{w_1}{w_3} \tag{3.25}$$

Thus, large values of $\dot{\epsilon}_{xx}$ create large Ra_1/Ra_3, which favors exponential growth. Conversely, if $\dot{\epsilon}_{xx}$ is small, perturbations should grow super-exponentially.

Both types of growth can be demonstrated by plotting $\ln(w')$, where w' is the dimensionless downward speed of the $T' = 0.9$ isotherm, as a function of the dimensionless time, t'. As discussed above, if growth is exponential, this curve should be linear, with slope equal to the dimensionless exponential growth rate, q'. For $Ra_1/Ra_3 = 10$

the approximately linear initial relationship between $\ln(w')$ and t', with an initial slope of 0.19 (Figure 3.3), agrees with measurements of $q' \sim 0.2$ made by *Conrad and Molnar* [1999] for Newtonian viscosity if $Ra_1 > 100$. Thus, for $Ra_1/Ra_3 = 10$, a perturbation initial grows exponentially with time. Later, the slope of this curve in Figure 3.3 increases, presumably because super-exponential growth begins to become important.

For $Ra_1/Ra_3 = 1$, a plot of $\ln(w')$ versus t' does not include an initial linear segment, but instead the slope rapidly increases with time (Figure 3.3). Growth in this case is super-exponential and the slope of a tangent to the curve of $\ln(w')$ versus t' gives a measurement of the "instantaneous" growth rate at a given time. The above theory predicts the value of this growth rate for a given perturbation amplitude. Taking the time derivative of (3.8), nondimensionalizing using the time scale for exponential growth in (3.5), and then simplifying using the definitions of Ra_1 and Ra_n in (3.20) and (3.21) yields:

$$\frac{dw'_n}{dt'} = nC^n \frac{Ra_n}{Ra_1} w'_n \tag{3.26}$$

Thus, the initial "instantaneous" slope of a plot of $\ln(w')$ versus t', denoted here as q'_0, should be equal to $nC^n Ra_n/Ra_1$. For $Ra_1/Ra_3 = 1$, a measurement of this initial slope using the first few data points gives $q'_0 = 0.45$ (Figure 3.3). This is larger than the predicted value of $nC^n Ra_n/Ra_1 = 0.27$, calculated using $C = 0.45$ [*Conrad and Molnar*, 1999], by nearly a factor of two. It is difficult, however, to fit a tangent to a set of points that are not linear, so perhaps an exact match to the theory should not be expected.

The transition from super-exponential to exponential growth can now be found by observing how measurements of q'_0 depend on Ra_1/Ra_3 (Figure 3.4). For large Ra_1/Ra_3 and exponential growth, the measured initial slope should be constant and equal to $q'_0 \sim 0.2$ (Figure 3.4) [*Conrad and Molnar*, 1999]. Although these measurements depend somewhat on perturbation size and begin to increase with increasing strain-rate for $Ra_1/Ra_3 > 100$, measured values of $q'_0 \sim 0.2$ are evident for

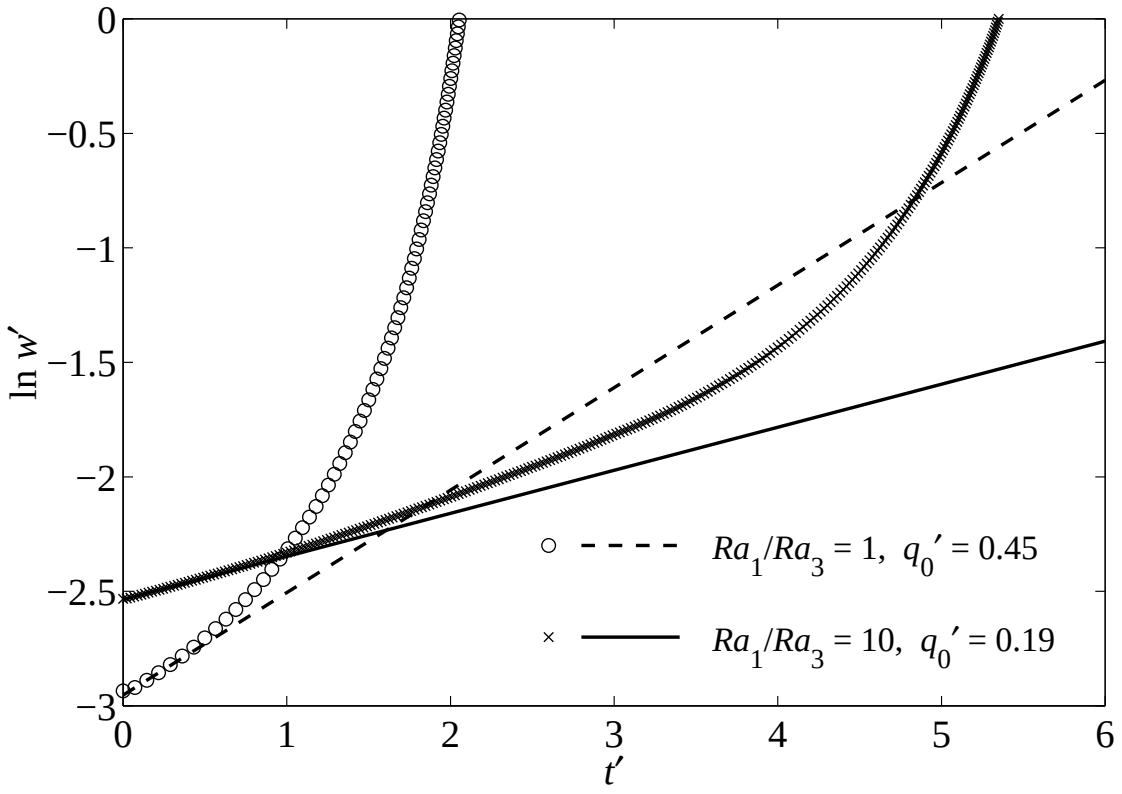

Figure 3.3: Plot of $\ln w'$, where w' is the downward speed of the $T' = 0.9$ isotherm, versus t' (nondimensionalized using (3.5) for exponential growth). Shown are curves for two choices of Ra_1/Ra_3 and for $r = 100$ and $Z_0' = 9.54\%$. Theory predicts that if growth is exponential, these curves should be linear, with slope equal to the dimensionless growth rate, q'. For $Ra_1/Ra_3 = 10$, the initially linear relationship indicates exponential growth with q' close to 0.2, the value expected for exponential growth [*Conrad and Molnar*, 1999]. Not even the initial part of the curve for $Ra_1/Ra_3 = 1$, however, is linear, but instead the "instantaneous" growth rate, as measured by the slope of a tangent to the curve at a given time, increases with time. This behavior is consistent with super-exponential growth of perturbations. The initial value of this "instantaneous" growth rate is estimated by measuring the average slope through the 2^{nd}, 3^{rd}, and 4^{th} data points. Because the initial slope changes rapidly with time, an accurate estimate of q' is difficult to make for super-exponential growth. By consistently measuring the slope in the same way, however, the variation of this initial "instantaneous" growth rate as a function of Ra_1/Ra_3 can be observed. This is shown in Figure 3.4, where the two growth rates measured here are marked.

$2 < Ra_1/Ra_3 < 100$. For small Ra_1/Ra_3, super-exponential growth should dominate even in initial stages. Indeed, for $Ra_1/Ra_3 < 2$ the measurements of q_0' follow the curve for nC^nRa_n/Ra_1 (Figure 3.4), as predicted by (3.26). These measured values are systematically larger, by about a factor of two, than the predicted values, as found for a single example in Figure 3.3, and can be attributed to the difficulty of measuring the true initial slope. The change in the dependence of q_0' on Ra_1/Ra_3 in Figure 3.4 indicates that the transition between super-exponential and exponential growth occurs for $Ra_1/Ra_3 \sim 2$. This value is independent of Z_0' and the temperature-dependence of B (Figure 3.4).

At sufficiently rapid background strain-rates, uniform thickening of the layer occurs faster than the gravitational instability grows. Thus, another transition, this one from exponential growth to uniform thickening, should occur as strain-rates increase. Again, this transition can be found by first taking the ratio of the speeds for mechanical thickening, w_s, and exponential growth, w_1, which can be simplified to:

$$\frac{w_1}{w_s} \sim \frac{Ra_1}{P} Z_0' \tag{3.27}$$

This ratio depends on the perturbation size Z_0' because the only important dimension affecting w_s in (3.12) is the layer thickness, but w_1 also increases with the size of the perturbation, as in (3.7). Thus, layers perturbed with different amplitudes should experience a transition from exponential growth to thickening at different values of Ra_1/P.

To see where thickening becomes important, measurements of q_0', the "instantaneous" initial growth rate discussed above, are plotted a function of $Z_0'Ra_1/P$ (Figure 3.5). If shortening is the most important growth mechanism, the downward speed at the base of a layer is given by w_s in (3.12). Taking the time derivative of (3.12), nondimensionalizing using (3.5), and simplifying using the definitions of Ra_1 and P in (3.20) and (3.22) yields:

$$\frac{dw_s'}{dt'} = \frac{P}{Ra_1} w_s' \tag{3.28}$$

Thus, if the layer grows only by thickening, $q_0' = P/Ra_1$. Measured values of q_0'

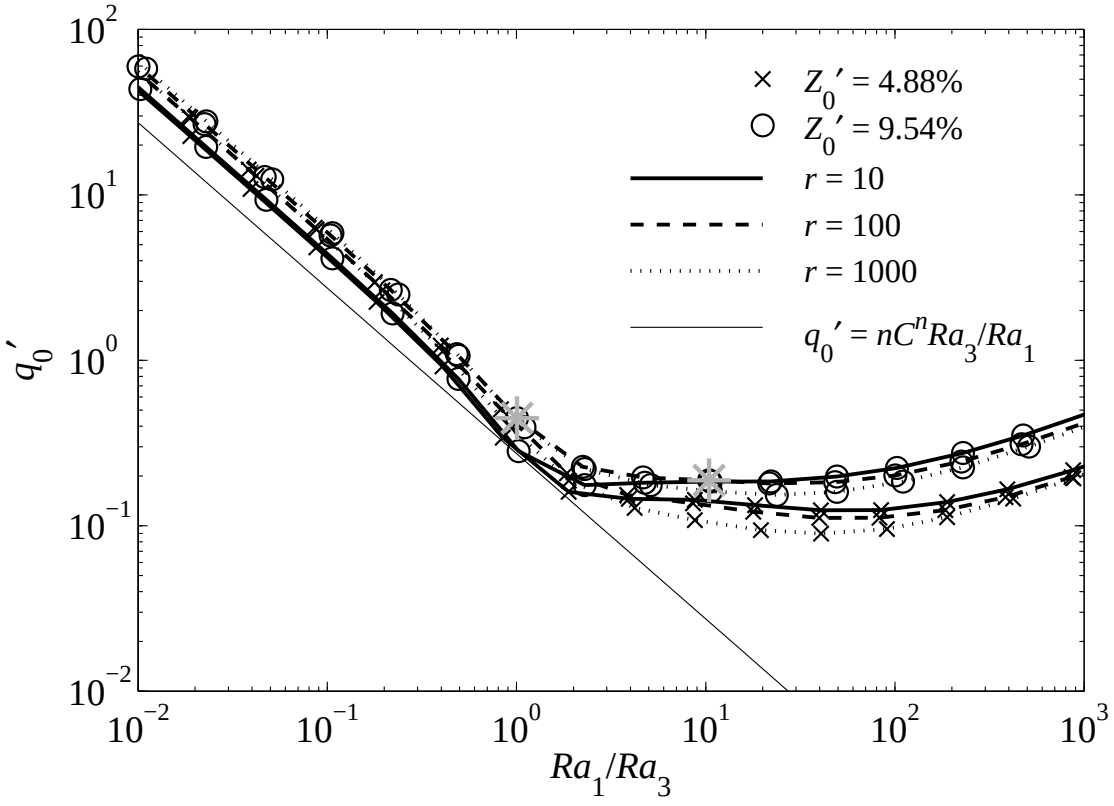

Figure 3.4: Plot of the initial dimensionless growth rate, q_0', as a function of Ra_1/Ra_3. Here q_0' is measured as shown in Figure 3.3 and where time is made dimensionless using (3.5). The smallest value of Ra_3 is 770 for the $Z_0' = 4.88\%$ and $r = 1000$ curve, meaning that the layer is always potentially unstable to super-exponential growth. This type of growth is observed for small strain-rates that produce $Ra_1/Ra_3 < 2$, where theory (see text) predicts super-exponential growth with initially $q_0' = nC^n Ra_3/Ra_1$ (thin solid line). For $Ra_1/Ra_3 > 2$, $q_0' \sim 0.2$, as predicted for exponential growth. Thus, for strain-rates that are large enough to produce $Ra_1/Ra_3 > 2$, the background viscosity of the layer is reduced sufficiently so that density perturbations grow unstably and exponentially with time. The large gray stars correspond to measurements made in Figure 3.3.

behave in this way for $Z_0' Ra_1/P < 0.5$ (Figure 3.5), for the three different initial perturbation amplitudes. For $Z_0' Ra_1/P > 0.5$, measured growth rates trend toward $q' \sim 0.2$. For small initial perturbations such as $Z_0' = 0.01$, growth rates may be smaller than $q' \sim 0.2$ even for $Z_0' Ra_1/P > 0.5$ (Figure 3.5), indicating that horizontal shortening still influences growth.

The transition between exponential and super-exponential growth, determined from Figure 3.4 to occur at $Ra_1/Ra_3 \sim 2$, can also be represented in terms of $Z_0' Ra_1/P$ and observed in Figure 3.5. By solving for the strain-rate at which $Ra_1/Ra_3 \sim 2$ and inserting this expression into the definition of $Z_0' Ra_1/P$ given in Table 3.1, it is possible to rewrite $Ra_1/Ra_3 \sim 2$ as $Z_0' Ra_1/P \sim 3.67 F_1 \sqrt{F_1/F_3}$. Using the values of F_1 and F_3 given by *Conrad and Molnar* [1999], the transition from exponential to super-exponential growth can be estimated to occur at $Z_0' Ra_1/P \sim 5$. This transition is evident Figure 3.5, and is, coincidentally, nearly independent of the temperature dependence of B across the layer.

3.4.4 Summary

Three dimensionless quantities, Ra_1, Ra_n, and P, together with the initial dimensionless perturbation size, Z_0', can be used to determine the mode of deformation that occurs in a cold thickening boundary layer with non-Newtonian viscosity and power-law exponent $n = 3$ (Table 3.1). If $Ra_3 > 100$, the instability may grow super-exponentially, but only if imposed strain-rates, $\dot{\epsilon}_{xx}$, are small enough that $Ra_1/Ra_3 < 2$ (Figure 3.4), or alternatively $Z_0' Ra_1/P > 5$ (Figure 3.5). If the imposed strain rate is large enough that $Z_0' Ra_1/P < 0.5$ (Figure 3.5), or alternatively $Ra_1/Ra_3 > 100$ (Figure 3.4), mechanical thickening of the layer dominates the downward advection of isotherms (Figure 3.5). Intermediate imposed strain-rates lead to exponential growth of perturbations, as long as $Ra_1 > 100$.

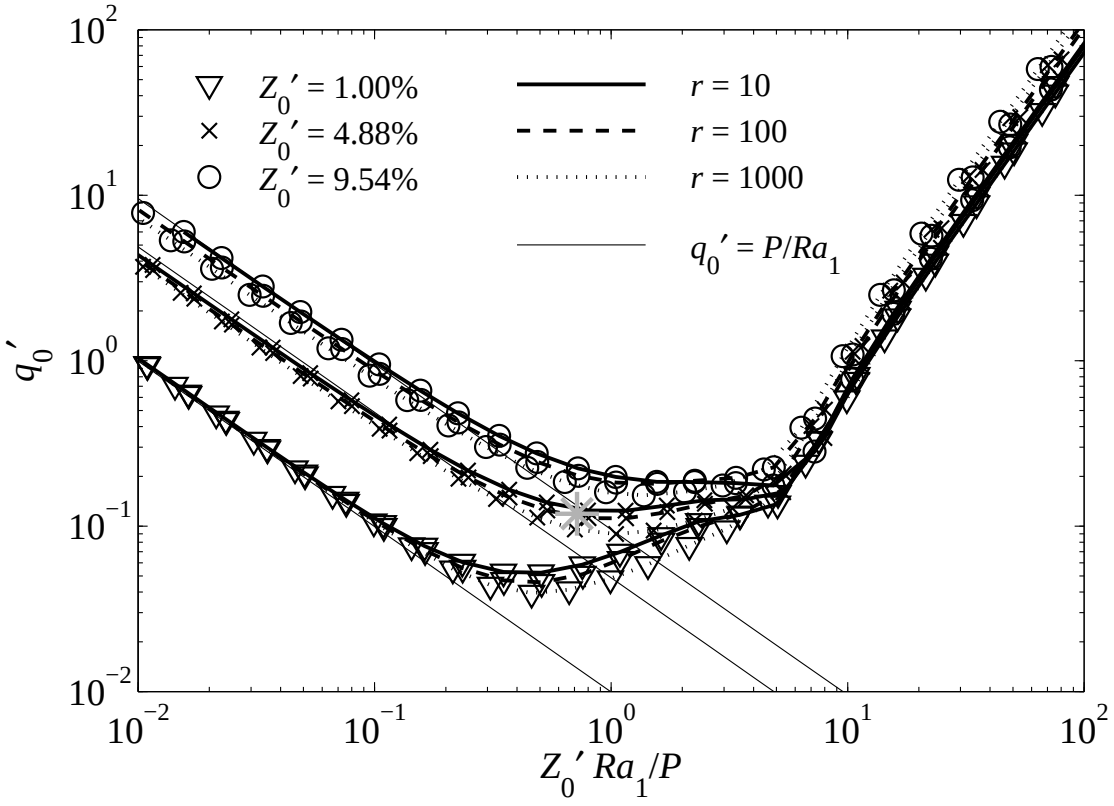

Figure 3.5: Plot of the initial dimensionless growth rate, q_0', made dimensionless using (3.5), as a function of $Z_0' Ra_1/P$. The results for which $Z_0' Ra_1/P > 5$ are the same as those for which $Ra_1/Ra_3 < 2$ in Figure 3.4, where they are attributed to super-exponential growth. Theory predicts (see text) that if growth is controlled by horizontal shortening, $q_0' = P/Ra_1$. This is observed for $Z_0' Ra_1/P < 0.5$ (compare to thin solid lines). For $0.5 < Z_0' Ra_1/P < 5$, a mixture of horizontal shortening and exponential growth causes growth rates to increase toward $q_0' = 0.2$, the value expected for exponential growth. The large gray star corresponds to a measurement made in Figure 3.6.

Table 3.1. Summary of Dimensionless Quantities (for $n = 3$)

Description of Dimensionless Quantity	Critical Values and Dominant Mode of Growth
$Ra_1 = \frac{\rho g \alpha T_0 h^3}{\kappa B_m} F_1 \dot{\epsilon}_{xx}^{2/3}$ Compares exponential growth and thermal diffusion	$Ra_1 > 100$ Exponential Growth $Ra_1 < 100$ No Growth
$Ra_3 = \left(\frac{\rho_m g \alpha T_0}{3B_m}\right)^3 \frac{h^3 Z^2}{\kappa} F_3$ Compares super-exponential growth and thermal diffusion	$Ra_3 > 100$ Super-Exponential Growth $Ra_3 < 100$ No Growth
$P = \frac{\dot{\epsilon}_{xx} h^2}{\kappa}$ Compares mechanical thickening and thickening due to cooling	Applies if $Ra_1 < 100$ and $Ra_3 < 100$ $P > 1$ Mechanical Thickening $P < 1$ Thickening due to Cooling
$\frac{Ra_1}{Ra_3} = 3\left(\frac{3B}{\rho g \alpha T_0 Z}\right)^2 \frac{F_1}{F_3} \dot{\epsilon}_{xx}^{2/3}$ Compares exponential growth and super-exponential growth	Applies if $Ra_1 > 100$ or $Ra_3 > 100$ $\frac{Ra_1}{Ra_3} < 2$ Super-Exponential Growth $2 < \frac{Ra_1}{Ra_3} < 100$ Exponential Growth $\frac{Ra_1}{Ra_3} > 100$ Mechanical Thickening
$Z' \frac{Ra_1}{P} = \frac{\rho g \alpha T_0 h}{\kappa B_m} F_1 \dot{\epsilon}_{xx}^{-1/3}$ Compares exponential growth and mechanical thickening	Applies if $Ra_1 > 100$ or $Ra_3 > 100$ $Z' \frac{Ra_1}{P} < 0.5$ Mechanical Thickening $0.5 < Z' \frac{Ra_1}{P} < 5$ Exponential Growth $Z' \frac{Ra_1}{P} > 5$ Super-Exponential Growth

3.5 Transitions Between Mechanisms of Instability

The dimensionless quantities Ra_1, Ra_3, and P depend on the layer thickness h, and thus increase as the layer thickens with time. The measure of instability Ra_3 also increases as gravitational instability grows because it depends on the perturbation amplitude Z. As a result, an unstable layer should experience transitions between different types of deformation as increases in h and Z cause Ra_1, Ra_3, and P to encounter the "critical" values described above and in Table 3.1.

As an example, consider convective instability at the base of a layer perturbed initially with amplitude $Z' = 4.88\%$, $r = 100$, and choices of $\dot{\epsilon}_{xx}$ and other parameters such that $Z'Ra_1/P \sim 0.7$. As noted in Figure 3.5 and shown by a plot of $\ln(w')$ versus t' (Figure 3.6a), such a layer undergoes a combination of Rayleigh-Taylor growth and horizontal shortening such that $q' = 0.12$, where time is made dimensionless using (3.5). This value is smaller than the value of $q' \sim 0.2$ appropriate for purely exponential growth. As discussed above and shown in Figure 3.5, however, $q' < 0.2$ for initial perturbation amplitudes that are sufficiently small because shortening still influences growth. Thus, in the example shown in Figure 3.6a, isotherms are initially advected downward in part by uniform thickening of the layer.

As the perturbation amplitude Z' increases with time due to Rayleigh-Taylor growth, the quantity $Z'Ra_1/P$ also increases, making deformation of the layer less influenced by mechanical thickening (Figure 3.5). In fact, transition to exponential growth occurs as the perturbation amplitude nears $Z' \sim 10\%$ and $Z'Ra_1/P$ nears 1.4 (Figure 3.6b), seen also in the change in slope near $t' = 2$ (Figure 3.6a). The new measured growth rate of $q' = 0.26$ is larger than expected for exponential growth. Because the layer has thickened by about 30% before exponential growth becomes dominant, however, the thickness h used in (3.5) to make time dimensionless should be increased by a factor of 1.3, making the value of 0.26 consistent with the predicted dimensionless growth rate of $q' = 0.2$ [*Conrad and Molnar*, 1999], and that observed in Figure 3.5 for $Z' = 10\%$ and $Z'Ra_1/P \sim 1.4$.

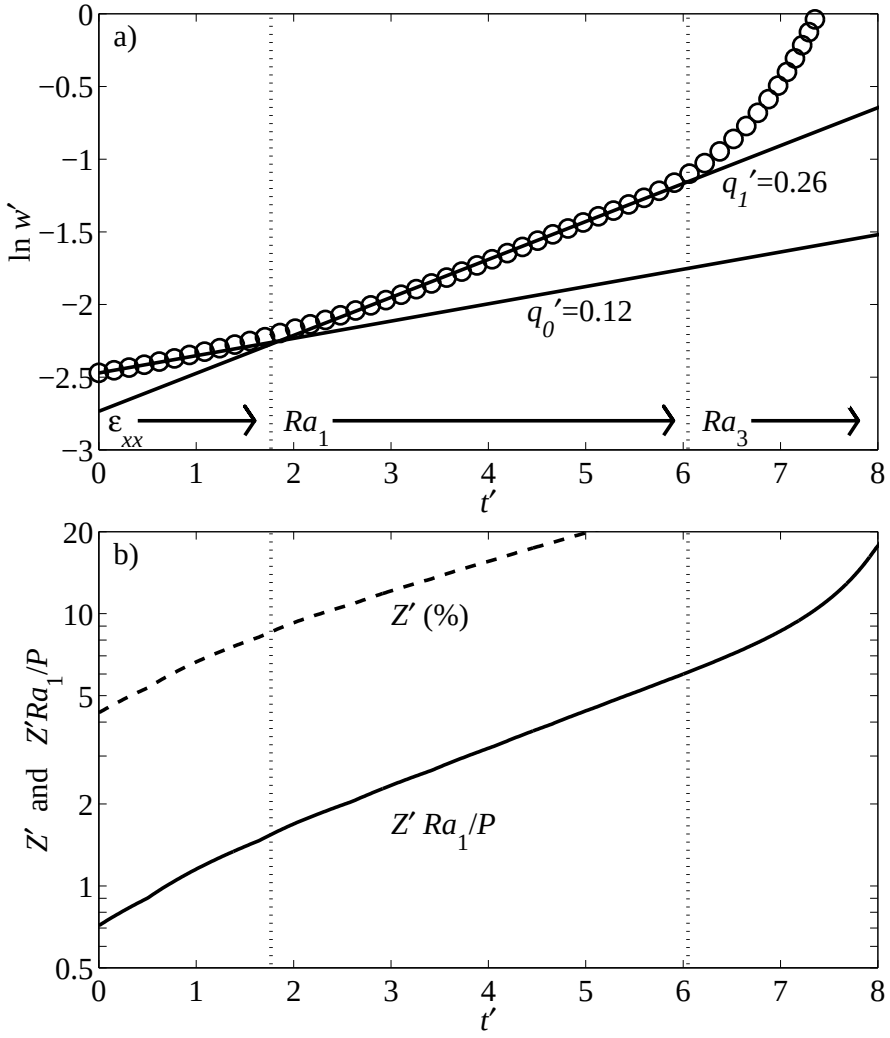

Figure 3.6: Plot of (a) $\ln w'$ as a function of time (made dimensionless using the time scale for exponential growth in (3.5)) for a layer with initial values of Ra_1, Ra_3, and P of 800, 10, and 50, respectively, and for $r = 100$ and $Z_0' = 4.88\%$. The time variation of the dimensionless perturbation amplitude Z' and the dimensionless parameter $Z'Ra_1/P$ is shown by (b). The linear trends in (a) show that growth is initially exponential, with growth rate $q' = 0.12$, until $Z'Ra_1/P \sim 1.4$, at which point the dimensionless growth rate increases to $q' = 0.26$. The slower initial growth can be attributed to the influence of the thickening rate, which initially moves isotherms downward faster than does exponential growth. When perturbations become sufficiently large ($Z' \sim 10\%$), exponential growth becomes fastest. Finally, super-exponential growth occurs for $Z'Ra_1/P > 5$. The transition between the various types of growth is approximately predicted by the changes in slopes in Figure 3.5, where the initial growth rate measurement of this calculation is marked.

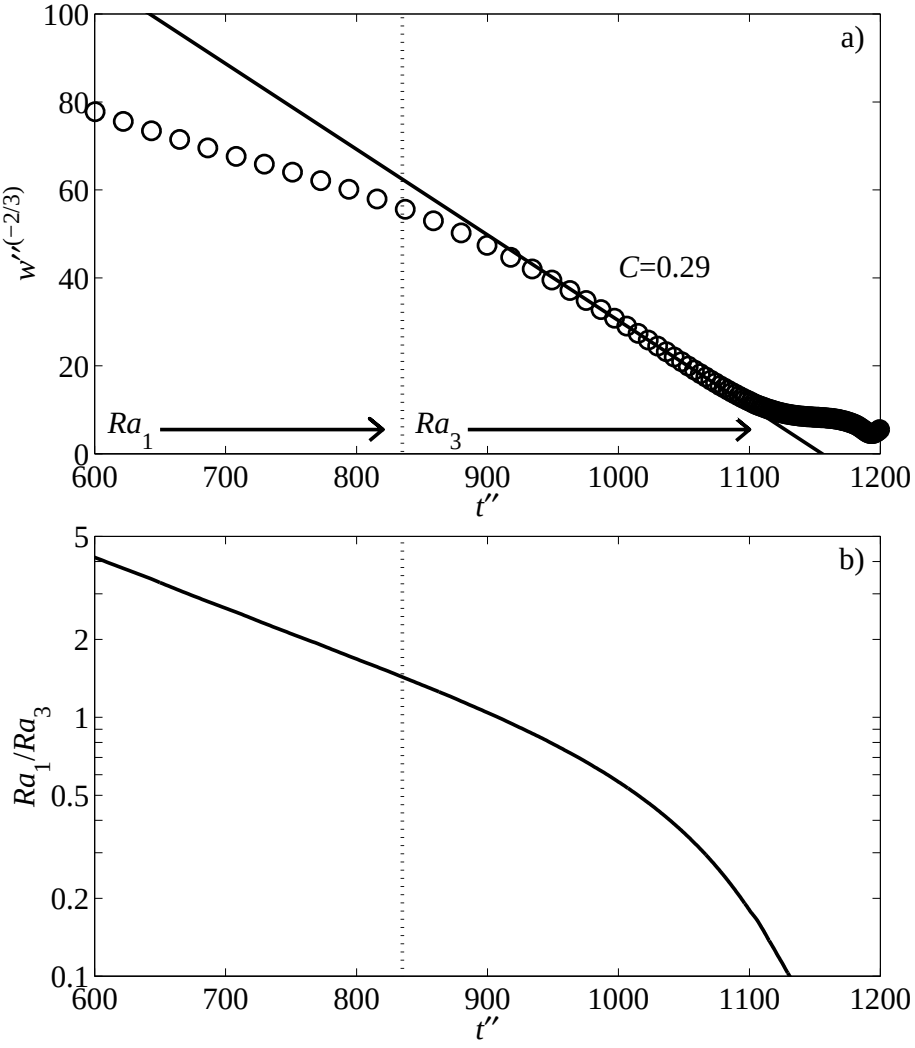

Figure 3.7: Plots of (a) $w''^{(-2/3)}$ and (b) the dimensionless parameter Ra_1/Ra_3, defined by (3.25), as a function of time (made dimensionless using the time scale for super-exponential growth in (3.9)) for the instability described in Figure 3.6. The linear behavior for $t'' > 840$ indicates super-exponential growth with growth parameter $C = 0.29$. This occurs when perturbation amplitudes become large enough that Ra_1/Ra_3 decreases below about 2, as shown in (b) and predicted in Figure 3.4. The line marking the approximate transition in behavior is the same as the one marked in Figure 3.6 for a different dimensionless time.

When perturbation amplitudes become sufficiently large that $Ra_3 > 100$ and $Ra_1/Ra_3 < 2$ (or if $Z'Ra_1/P > 5$), super-exponential growth of perturbations is faster than exponential growth. In Figure 3.6, where time is nondimensionalized using the time scale for exponential growth given by (3.5), growth becomes faster than exponential for $t' > 6$, the time at which $Z'Ra_1/P \sim 5$ (Figure 3.6b), consistent with the transition in Figure 3.5. This same time is marked in Figure 3.7 at $t'' \sim 840$, where time is nondimensionalized using the time scale for super-exponential growth given by (3.9). For $t'' > 840$, the plot of $w''^{(-2/3)}$ versus t'' is approximately linear, with slope indicating a growth parameter of $C = 0.29$ (Figure 3.7a). This transition to super-exponential growth occurs when Ra_1/Ra_3 becomes less than about 2 (Figure 3.7b), the critical value of this ratio in Figure 3.4. The measured value of $C = 0.29$ is smaller than the value of $C \sim 0.4$ measured by *Conrad and Molnar* [1999]. This discrepancy is exacerbated by the fact that the layer has thickened by about 70% when super-exponential growth begins, meaning that this measured value should be reduced further by a factor of $(1.7)^{1/n} = 1.2$, as determined by the relationship between h and C in (3.8). *Conrad and Molnar* [1999], however, measured C using an initial perturbation amplitude only 10% of h. Here super-exponential growth is measured from a layer that has been previously distorted at large amplitudes by both thickening and exponential growth. If the resulting perturbation structure is not optimal for growth, these perturbations might grow more slowly than those measured by *Conrad and Molnar* [1999].

For a thickening unstable layer, the dominant mode of deformation progresses from exponentially increasing mechanical thickening, to faster exponential growth of a gravitational instability, and finally to still faster super-exponential growth of this instability. Depending on initial conditions, these three types of deformation will evolve from one to the next as the layer thickens and perturbations grow. The scaling analysis developed above for an initially perturbed layer can be used to predict the approximate time-dependent evolution of a thickening unstable layer that experiences transitions between different styles of thickening and growth as it evolves.

3.6 The Evolving Thermal State of an Unstable Layer

If mechanical thickening of mantle lithosphere generates convective instability, the lithosphere's low viscosity basal portion will be removed in an event whose time dependence is described above. The colder, more viscous shallow lithosphere may also be unstable, but on time scales longer than those that apply to the initial lower lithosphere instability [*Molnar, Houseman and Conrad*, 1998]. Thus, convective erosion at the lithospheric base should continue at progressively slower rates until the layer is thin enough to be convectively stable, as defined by $Ra_3 < 100$. Complete convective stability, however, is not likely to be achieved for billions of years following an initial instability [*Conrad and Molnar*, 1999], perhaps making stability geologically unimportant. Instead, the actual amount of material removed by convective instability and the subsequent convective erosion depends on the time scale relevant to the geologic process that is being studied.

Previous studies of convective instability [e.g., *Conrad and Molnar*, 1999; *Molnar, Houseman and Conrad*, 1998] extrapolate the analysis for a single downwelling instability to the ongoing convective erosion of a layer afterwards. As a result, they do not account for the ongoing thermal evolution of the layer due to heating by the influx of hot asthenosphere from below, or additional cooling from above. In addition, they ignore the possible role that ongoing horizontal shortening may play in continuing to thicken the layer. To study the evolution of mantle lithosphere after its base is convectively removed, calculations similar to those described above are extended for times beyond this initial event.

3.6.1 Additional Numerical Calculations

In the lithosphere, shortening, and therefore convective instability caused by shortening, occurs at convergent zones between large plates of nearly constant thickness. To consider durations of convergence long enough to allow large finite shortening, I

extend the width of the finite element grid to $6.20h$, three times that used in the calculations above. The wider grid allows the instability to occur farther from the right edge where imposed boundary conditions generate shortening, and thus should diminish the influence of these boundary conditions on the evolution of the shortening region after the instability occurs. Shortening is permitted only in the left one-third of the grid by adding uniform velocity boundary conditions to the top surface of the rightmost two-thirds of the grid. Thus, at the surface, the horizontal velocity tapers unformly from zero to $-v$ on $0 < x' < 2.07$ and is equal to $-v$ on $2.07 < x' < 6.20$. The other boundary conditions are the same as those used above.

The imposed horizontal shortening causes the unstable layer to thicken at a rate that can be expressed by P using (3.22) as a multiple of the thermal diffusion time scale. Perhaps a more meaningful expression for the thickening rate is the time for a layer's thickness to increase by 100%. In these calculations, a doubling of layer thickness can be achieved by collapsing a region of width $2L$ into a region of width L, which corresponds to horizontal shortening of 50%. If L is the width of the shortening region and material is brought into this region with velocity v, then the horizontal strain-rate is $\dot{\epsilon}_{xx} = v/L$ and 100% thickening is achieved after a time $t_{100} = L/v = 1/\dot{\epsilon}_{xx}$. Using (3.22), t_{100} can be written in terms of P:

$$t_{100} = \frac{1}{\dot{\epsilon}_{xx}} = \frac{h^2}{P\kappa} \tag{3.29}$$

Later, it will be useful to make time nondimensional using the time scale for exponential growth. Applying (3.5) and simplifying yields:

$$t'_{100} = \frac{Ra_1}{P} \tag{3.30}$$

Values for P and Ra_1 are given below so that t'_{100} can be calculated using (3.30).

Sixteen calculations are performed, for four different temperature dependences of viscosity, given by values of r of 1, 10, 100, and 1000, and for four different shortening rates, which yield values of P of 1.5, 4.8, 15, and 48. Because the stability parameter Ra_1 depends on strain-rate, as shown by (3.20) and (3.3), layers with larger values

of P, and thus larger strain-rates, have larger Ra_1, making them convectively more unstable. To study layers that are inherently stable when subject to low shortening rates, but that become unstable when shortening rates increase, the strength parameter B_m is chosen so that a layer shortening with $P = 4.8$ has a value of Ra_1 near the critical value of 100. Because layers with larger r, and therefore smaller "available buoyancy" parameter F_1, have a diminished tendency toward convective instability (as shown by (3.20)), the chosen values of B_m are smaller for layers with larger r. Thus, despite differences in r, layers are equally unstable at a given shortening rate. The stability parameter Ra_1 is thus varied only by changing the shortening rate, which is specified here by a change in P.

Because horizontal shortening is only imposed between $x' = 0$ and 2.07, thickening in this region generates a perturbation to the initially unperturbed error-function temperature profile. This perturbation then should grow unstably, either exponentially with time if shortening is sufficiently rapid that $Ra_1 > 100$, or super-exponentially with time once this perturbation becomes large enough that $Ra_3 > 100$. Either way, localized thickening eventually leads to a perturbation that grows unstably. This initial downwelling eventually removes the basal portion of the layer, as shown for $r = 100$ by the locations of isotherms in Figure 3.8 (black lines). Typically, downwelling persists following the initial removal event, and continues to remove cold material from both the upper reaches of the surface layer, as well as new material that is brought in from the side. This downwelling appears to be a permanent feature and eventually reaches a steady state in which it removes all new cold material that is brought in by the imposed horizontal shortening (Figure 3.8, grey lines).

3.6.2 The Evolution of Downwelling

To study the instability's development over time, I record the locations and downward speeds of the nine isotherms between $T' = 0.1$ and $T' = 0.9$ on left side of the box, where the instability is a maximum. I also record the depth of these isotherms as they are advected into the right-hand side of the box. The amplitude of the perturbation to each isotherm, Z', can be measured by taking the difference in an isotherm's depth

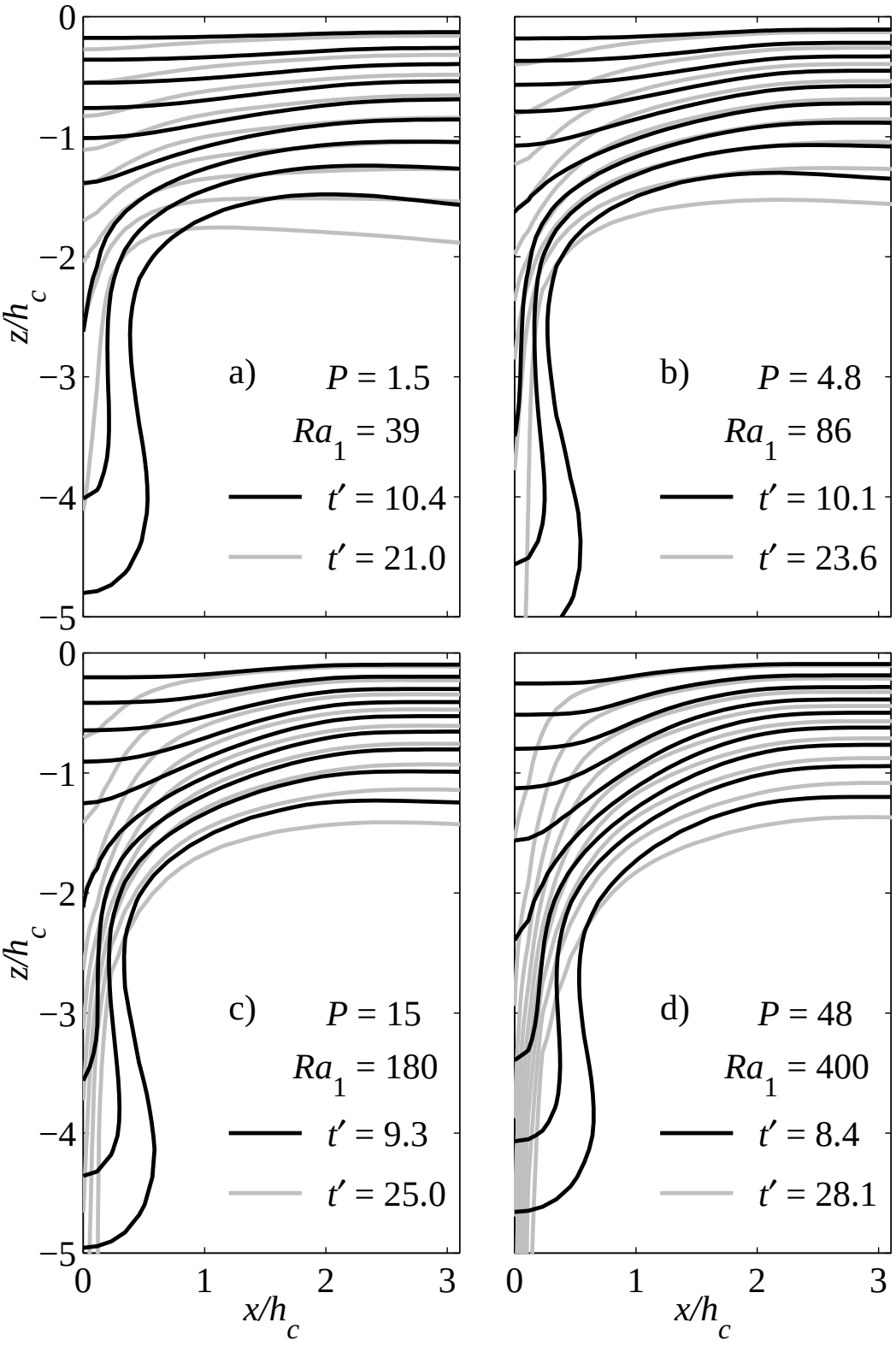
a)
P = 1.5
Ra1 = 39
t′ = 10.4
t′ = 21.0
b)
P = 4.8
Ra1 = 86
t′ = 10.1
t′ = 23.6
c)
P = 15
Ra1 = 180
t′ = 9.3
t′ = 25.0
d)
P = 48
Ra1 = 400
t′ = 8.4
t′ = 28.1
z/hc
x/hc
0
−1
−2
−3
−4
−5
1
2
3

Figure 3.8: Profiles of temperature for a convective instability growing from a thickening thermal boundary layer with temperature-dependent, non-Newtonian viscosity for which $n = 3$ and $r = 100$. Only the left half and the upper 60% of the entire finite element calculation is shown. Growth is initiated by imposing velocity boundary conditions on an initially unperturbed error function temperature profile. These boundary conditions generate horizontal shortening between $x' = 0$ and $x' = 2.06$, as described in the text. Thus, the layer thickens in this region, which generates a lateral variation in the temperature field from which convective instability can grow. Shown are isotherms for $T' = 0.1$ through 0.9, with colder temperatures closer to the surface. Sets of isotherms for different shortening rates are shown in parts (a) through (d), where the difference in shortening rates is parameterized by P, but also affects Ra_1 by changing the background viscosity of the layer. In each case, two times are shown, where time is nondimensionalized using the time scale for exponential growth given by (3.5). The dark contours show a time during the super-exponential phase of the instability, in which a "blob" of material is rapidly descending into the lower halfspace. The light contours show the instability at the end of the calculation, when cold material is flowing downward from the base of the instability at a nearly steady rate.

between the left and right hand sides of the grid, and then normalizing this quantity by the original depth of that isotherm. To determine the fraction of the downward speed that is not due to the initially-imposed velocity field associated with horizontal shortening, the initial speed of material containing a given isotherm is subtracted from its measured value. Because the layers are initially unperturbed, this initial speed should result almost entirely from horizontal shortening. The velocity that remains, termed w'_{corr} here, must be associated with either gravitational instability or the acceleration of mechanical thickening beyond its initial rate (remember that w_s in (3.12) grows exponentially with time).

A comparison of the expressions for w_1 and w_n in (3.7) and (3.8), shows that if gravitational instability dominates, a plot of $\ln(w'_{corr})$ versus $\ln(Z')$ should yield a linear relationship with slope equal to the power-law exponent, n, that depends on the style of growth: $n = 1$ for exponential and $n > 1$ for super-exponential growth [*Molnar, Houseman and Conrad*, 1998]. If mechanical thickening dominates, subtracting the initial velocity from (3.12) yields $w_{corr} = \dot{\epsilon}_{xx} Z$ if $h(t) = h(t = 0) + Z(t)$. This

relation should, like exponential growth, yield a slope of unity in a plot of $\ln(w'_{corr})$ versus $\ln(Z')$. Such a plot (Figure 3.9) shows a slope near unity for the coldest isotherms, indicating exponential growth of perturbations or mechanical thickening throughout. For the hotter isotherms, a change in slopes indicates a transition to super-exponential growth of perturbations (slope of $m = n = 3$). For all of the calculations shown in Figure 3.9, the dimensionless quantity $Z'Ra_1/P > 0.5$ for $Z' > 6\%$ ($ln(Z') > -2.8$ in Figure 3.9). This implies that exponential growth (rather than horizontal shortening) dominates prior to the transition to super-exponential growth, at least for the hotter isotherms. Following this period of super-exponential growth, curves for the hotter isotherms begin to oscillate due to an interaction with the base of the finite element grid (Figure 3.9), indicating that these isotherms have detached from the cold surface layer.

Thus, growth for the hotter isotherms is initially exponential, but that soon becomes super-exponential and eventually leads to the removal of the basal portion of the layer. The time for this removal to occur once the super-exponential growth phase begins can be estimated using (3.11), where time is nondimensionalized using (3.9) for super-exponential growth. Changing this nondimensionalization to that of exponential growth using (3.5) yields:

$$t'_b = \frac{1}{(n-1)C^n}\frac{Ra_1}{Ra_n} \tag{3.31}$$

If $n = 3$, super-exponential growth begins when $Ra_1/Ra_3 \sim 2$. Using this value and $C = 0.45$, the time to the initial removal event can be estimated as $t'_b \sim 11$, and is independent of shortening rate. This is comparable to the times shown in Figure 3.8 for the initial instability to become large (times associated with black curves), but allows no time for the development of perturbations prior to the initiation of super-exponential growth. The estimates of $Ra_1/Ra_3 = 2$ and $C = 0.45$ are, however, approximate. If instead $Ra_1/Ra_3 \sim 1.5$ is appropriate, as it seems to be in Figure 3.7b, $t'_b \sim 8$, a value that is nearly as large as the times shown in Figure 3.8. Thus, the initial removal event consists primarily of a super-exponential growth phase, but is

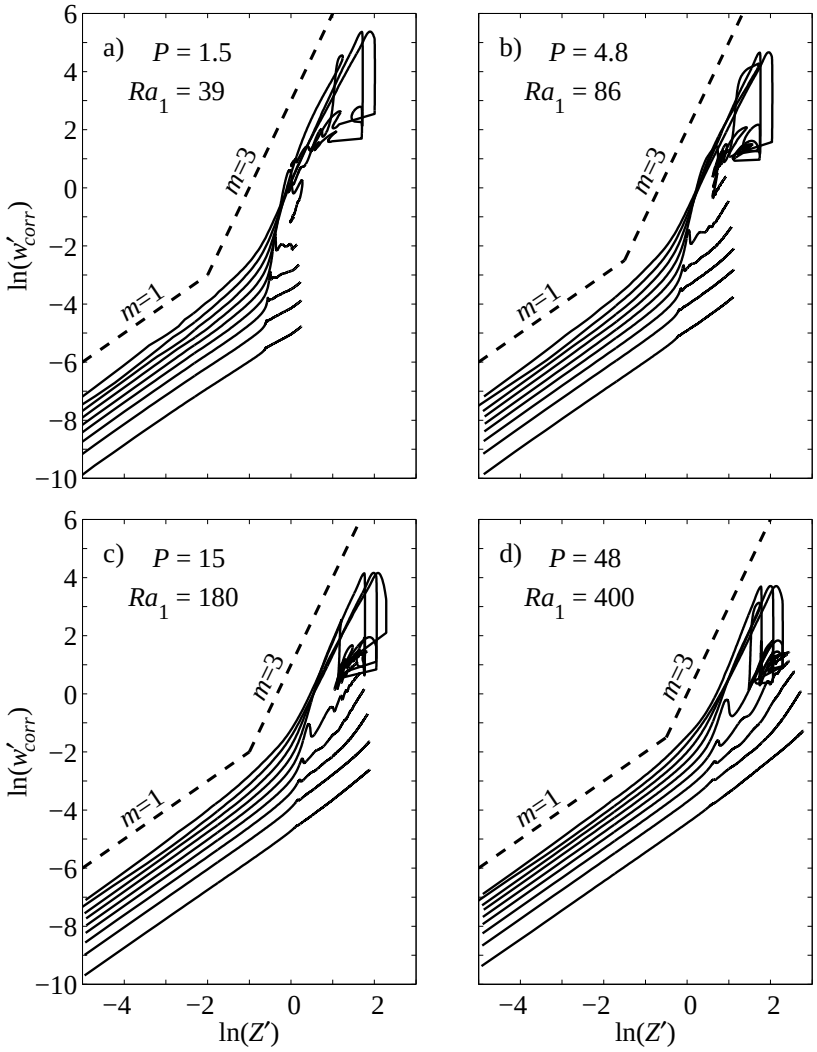

Figure 3.9: A plot of $\ln(w'_{corr})$ as a function of $\ln(Z')$ for each of the nine isotherms (solid lines, $T' = 0.1$ through 0.9) and for the four calculations shown in Figure 3.8 (parts (a) through (d)). The colder isotherms have smaller initial velocities. Here $w'_{corr} = w' - w'(t = 0)$ and Z' are measured as described in the text. As shown by taking the natural log of the expression for exponential growth of gravitational instability in (3.7) or the corrected expression for horizontal shortening (see text), a slope of $m = 1$ indicates that one of these two modes is dominant. By taking the natural log of equation (3.8), a slope of $m = 3$ indicates super-exponential growth for power-law creep with exponent $n = 3$. Dashed lines with slopes of 1 and 3 are shown for comparison. Initially, all of the isotherms experience either exponential growth of gravitational instability or mechanical thickening (slope of 1). Eventually, the hotter isotherms are removed by an event in which perturbations grow super-exponentially with time (slope of 3). These isotherms later cease their growth because they fall through the bottom of the box and begin a period of oscillatory behavior.

preceded by a brief exponential growth phase, and perhaps an even briefer horizontal shortening phase. Because the dimensionless duration of super-exponential growth is independent of the shortening rate, the slightly shorter times for faster shortening rate (larger P in Figure 3.8) can be attributed to the dependence of the exponential growth phase's duration on shortening rate. If shortening is faster, less time is spent in the generation of perturbations large enough to produce $Ra_3 > 100$, the condition for initiation of super-exponential growth.

3.6.3 The Thermal State After Initial Instability

The amount of material removed by the initial instability can be estimated by observing the number of isotherms that participate in the initial downwelling in Figure 3.8. For example, the bottom three isotherms are clearly involved in the downwelling for the slowest shortening rate (Figure 3.8a). A fourth isotherm appears to join the instability for faster shortening (Figure 3.8d). Another way of determining how much material is initially removed is to estimate how many isotherms change their slopes from $m = 1$ to $m = 3$ in Figure 3.9. It is clear that the colder isotherms (smaller w') do not change slope, except for a small, temporary, acceleration that occurs when the hotter isotherms begin their super-exponential phase. In each of the four cases shown in Figure 3.9, the hotter four isotherms change their slope significantly, while perturbations to the colder five isotherms continue with slopes near unity. The initial removal event is also evident in a plot of the depth of each isotherm as a function of time (Figure 3.10), and it is clear that between three and four isotherms are removed by it.

A more quantitative estimate of the amount of material removed by the initial instability can be obtained by examining the distribution of isotherms at the removal time in Figure 3.10. In particular, the ratio of each isotherm's depth at a given time to its initial depth defines a "thickening factor" that can then be used to compare the relative deflections of different isotherms at various times. At the removal time, defined here to be the time in which the $T' = 0.9$ isotherm first encounters the bottom boundary of the finite element grid, isotherms are typically separated into two groups.

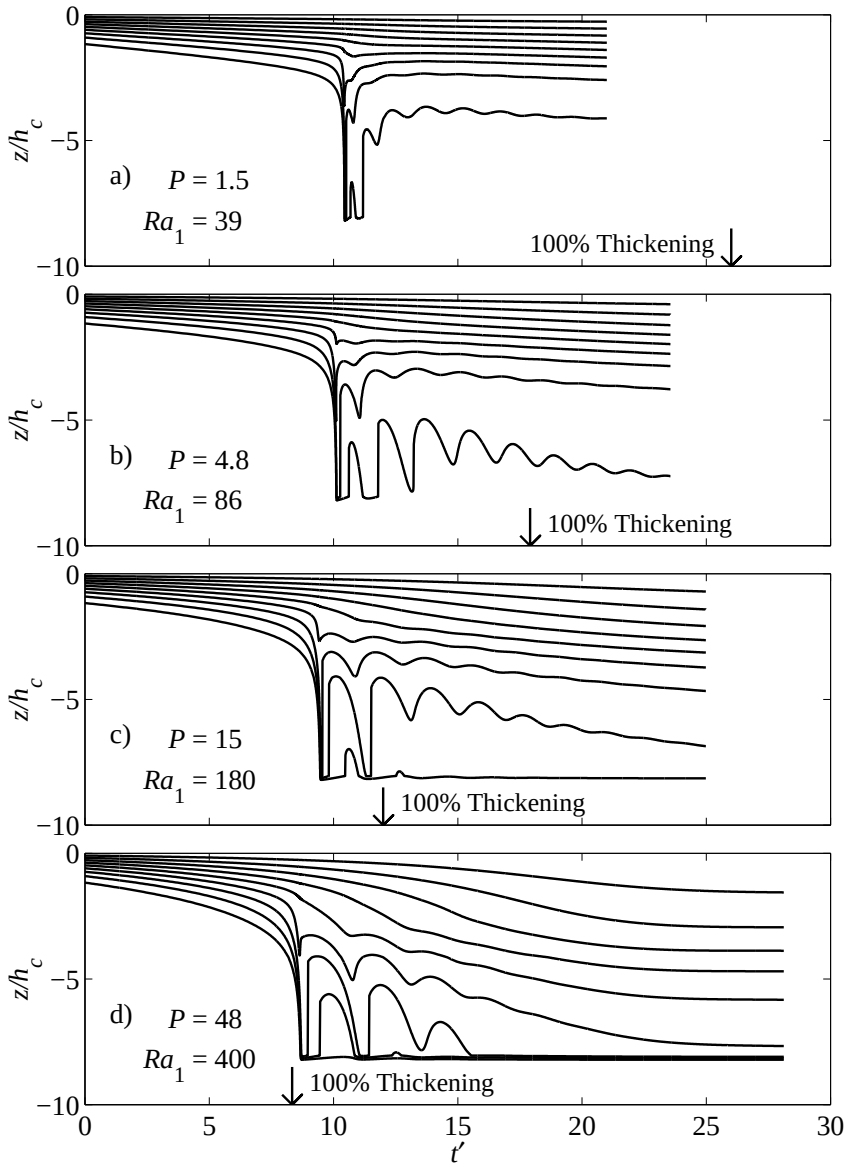

Figure 3.10: A plot showing the depth of each of the nine isotherms ($T' = 0.1$ through 0.9, where the colder isotherms are closer to the surface), as a function of time (made dimensionless using the time scale for exponential growth in (3.5)) for the four calculations shown in Figure 3.8 (parts (a) through (d)). In each case, the super-exponential growth phase is evident as the bottom isotherms plunge deeply into the lower halfspace, eventually descending through the base of the grid at $z' = 8.27$. These isotherms then begin a period of oscillatory behavior while the shallower isotherms continue to be drawn downwards. Also shown for each case is the dimensionless time at which the layer would have thickened by 100% in the absence of convective instability. This time corresponds to 50% shortening at the surface and is given by (3.30) as $t'_{100} = Ra_1/P$.

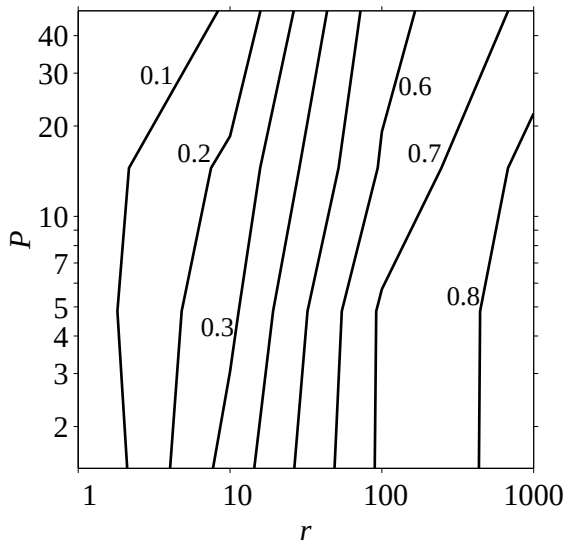

Figure 3.11: A plot showing, as a function of shortening rate (expressed by P) and the temperature dependence of viscosity (expressed by r), the dimensionless temperature of the coldest material removed by the first, super-exponential growth removal event. This temperature is defined as that of material that deepens to a depth 5 times greater than its original (unperturbed) depth at the time of the initial instability. It is evident that a greater portion of the layer is initially removed if viscosity is only weakly temperature-dependent (smaller r) and that the shortening rate has little effect on the amount of material removed in this initial event.

Colder isotherms subside steadily with time (Figure 3.10) and typically deepen by a factor less than about 3 by the time of the removal event. Hotter isotherms that actively participate in this event penetrate deeply into the box, which causes them to grow deeper by factors greater than about 7, a quantity limited by the box depth (Figure 3.10). The isotherm that delineates the boundary between these two types of behavior can be defined as the temperature of material for which an arbitrarily chosen thickening factor of 5 applies (Figure 3.11). The factor of 5 is midway between the values of 7 and 3 estimated for isotherm "removal" and "nonremoval," but tests show that choosing 4 or 6 gives similar results.

The approximate temperature of the coldest material that participates in the initial removal event is shown in Figure 3.11. For example, the $T' \sim 0.7$ isotherm is removed for $r = 100$, with slightly colder material being removed at higher short-

ening rates (Figure 3.11). This estimate is supported by comparing the deflection of the $T' \sim 0.7$ isotherm to that of the other isotherms in Figure 3.10. The cutoff temperature for removal (Figure 3.11) is highly dependent on the temperature dependence of viscosity coefficient, r, with nearly the entire layer being initially removed in the constant B case ($r = 1$), and only the bottom few isotherms being removed if $r = 1000$. As found above for $r = 100$, the amount of material removed in this initial removal event does not depend strongly on the rate of shortening. This is due to the domination of the initial removal event by super-exponential growth, which, unlike exponential growth, does not depend on the shortening rate. Thus, the shortening rate should not affect the amount of material removed in this *initial* instability, provided this rate is large enough to generate instability.

3.6.4 The Thermal State After Prolonged Thickening

Because these calculations extend beyond the initial instability, they can be used to examine deformation of the unstable layer after the initial removal event. As the initial downwelling passes through the base of the finite element grid, the negative thermal buoyancy associated with the downwelling isotherms is suddenly removed, which causes these isotherms to retreat rapidly. This response is typically followed by another advance of downwelling, and oscillatory behavior develops (Figure 3.10) until it is damped into a steady state downwelling flow (Figure 3.8). Several colder isotherms that do not participate in the initial removal event are eventually drawn into this later downwelling flow (Figure 3.8). The slope of $m \approx 1$ in Figure 3.9 indicates that they descend either by exponential growth of gravitational instability or by continued mechanical thickening.

A layer's tendency toward exponential growth of gravitational instability is measured by Ra_1, which, because it depends on the layer's background viscosity, and thus its background shortening rate, increases with P. Thus, faster shortening rates cause both P and Ra_1 to increase (remember that, for a given value of r, Ra_1 is changed only by varying the shortening rate). Thus, if the observed long-term instability is due to exponential growth, downwellings should be more substantial at larger strain-

rates because greater Ra_1 enhances instability. This is indeed what the calculations show. For example, if P (and thus Ra_1) is small, only the bottom few isotherms are significantly deflected at the end of the calculation (Figure 3.8a), but nearly all of the dense layer is removed at fast shortening rates (Figure 3.8d). In addition, the colder isotherms penetrate more deeply (Figures 3.9 and 3.10) at faster shortening rates (larger P).

The same behavior, however, might also result from mechanical thickening of the cold part of the layer. The velocity boundary conditions force cold fluid into the right side of the finite element grid and out through its bottom. If the cold surface layer is in thermal steady state, this cold fluid must be removed from the layer by the persistent downwelling. In this light, it is not surprising that increased shortening rates are associated with a more substantial downwelling that penetrates deeper into the underlying fluid. The depth of penetration of these isotherms can be estimated by comparing the final depth of each isotherm to that isotherm's initial depth. The average of this "deepening factor" for the isotherms that do not encounter the bottom of the box at the end of the calculation provides a measure of how deeply a downwelling extends below the shortening region at the surface (Figure 3.12a). Downwellings are more substantial for rapidly shortening layers (expressed by P), but the amount of material that participates in these downwellings depends only weakly on the temperature-dependence of viscosity (expressed by r). This indicates that these downwellings serve as a mechanism by which thickened material can be continuously removed from a shortening layer. Although this process is generated by shortening, it is facilitated by the inherent gravitational instability of this material, which causes it to ultimately be removed by active downwelling.

The gravitational removal of the basal part of the surface layer prevents it from thickening into an overly unstable condition from which another transient instability can develop. Thus, the persistent downwellings that follow prolonged shortening are part of the steady-state behavior of a shortening layer. In the Earth, however, shortening cannot be expected to continue indefinitely. If shortening ceased, some, at least, of the material protruding into the asthenosphere would presumably become

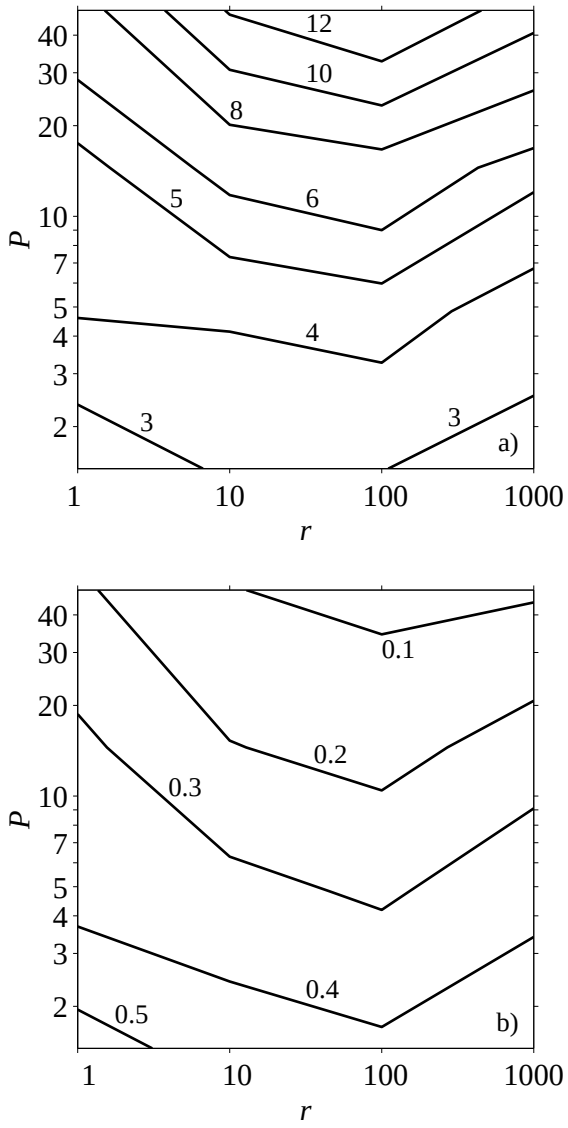

Figure 3.12: Similar to Figure 3.11, but showing the thermal properties of the steady-state persistent downwelling that removes material added to the layer by shortening. (a) shows the approximate depth to which this downwelling penetrates at the end of the calculations, expressed as a multiple of the original depth of the layer. This depth is calculated by taking the average of the factor by which each of the nine isotherms between $T' = 0.1$ and 0.9 deepens, excluding the isotherms that encounter the bottom of the box at that time. (b) shows the temperature of downwelling material at a depth equal to that of the original position of the $T' = 0.9$ isotherm. If shortening were to stop at this point, material hotter than that shown in (b) would presumably be removed. It is clear that the persistent downwelling advects cold material deeper into the mantle if the shortening rate is higher (larger P), and that the temperature dependence of viscosity is of lesser importance.

unstable, detach, and then be replaced by hotter material. The amount of material that might be removed can be estimated by measuring the temperature of the coldest material that protrudes deeper than the original depth of the $T' = 0.9$ isotherm, taken to represent the base of the unstable layer. These temperatures are shown in Figure 3.12b for a downwelling in thermal steady-state. It is clear that colder material is removed from more rapidly shortening layers (large P), but that the temperature of material removed is independent of the temperature-dependence of viscosity. This is consistent with more rapid shortening producing more substantial persistent downwellings, which are subject to removal once shortening stops.

3.6.5 The Thermal State After 50% Shortening

Geological observations in severely shortened regions such as Tibet indicate that the total amount of horizontal shortening can reach 50% (shortening by a factor of two) [*Le Pichon, Fournier, and Jolivet*, 1992; *Molnar, England, and Martinod*, 1993]. Horizontal shortening of this magnitude can be accommodated by a doubling of crustal thickness (100% thickening) in the shortening region, which generates significant buoyancy that resists further crustal thickening. This resistance causes the region of active shortening to migrate to undeformed adjacent regions once horizontal shortening has reached about 50% [e.g., *England and Houseman*, 1986; *England and Searle*, 1986; *Molnar and Tapponnier*, 1978]. If the amount of horizontal shortening is limited to 50%, the amount of time that dense mantle lithosphere is exposed to the destabilizing effects of horizontal shortening is also limited. In this case, the persistent downwellings discussed above might not penetrate as deeply as they would if allowed to grow indefinitely.

Because the dimensionless time to the initial removal event is a constant value of about 8, 50% shortening occurs well after the initial removal event for a slowly shortening layer (Figure 3.10a), but the two may be nearly simultaneous if shortening is rapid (Figure 3.10d). Thus, for the shortening rates studied, 50% shortening typically occurs sometime after the initial removal event, but before the persistent downwelling has grown to its full extent. To characterize the thermal state of the persistent down-

welling at the time of 50% shortening, the depth of penetration of an isotherm at the time t'_{100} is calculated and expressed as a multiple of the original depth of the layer. This calculation is similar to the one performed above for the downwelling after prolonged thickening, but includes only those isotherms that are not removed in the initial removal event. Because, for $r = 1$, all isotherms participate (Figure 3.10), only the coldest three isotherms are used. The result (Figure 3.13a) shows that persistent downwellings are generally less substantial for 50% shortening than they are for prolonged shortening (Figure 3.12a), particularly at large strain-rates. In fact, their diminishment at large P means that for $r > 10$, the deepening factor has a nearly constant value between 3 and 4 (Figure 3.13a). Downwelling of this magnitude causes material hotter than a dimensionless temperature T' between 0.3 and 0.4 to protrude deeper than the original depth of the $T' = 0.9$ isotherm (Figure 3.13b). Thus, if convergence slows after shortening an unstable layer by 50%, the hottest 60 to 70% of downwelling fluid should be removed. This fraction does not depend significantly on shortening rate or on the temperature dependence of viscosity.

3.7 Application to the Lithosphere

The above analysis shows that several styles of deformation are possible for a dense layer undergoing horizontal shortening, and that the particular style that a layer chooses depends on the values of the dimensionless quantities Ra_1, Ra_3, P, and Z'. This analysis can now be applied to the mantle lithosphere to determine the types of deformation that are possible as a result of shortening, and to characterize the changes to the lithospheric structure that may result from this deformation. To do this, parameter values relevant to the lithosphere must be estimated. These include $\rho_m = 3300$ kg m^{-3}, $g = 9.8$ m s^{-2}, $\alpha = 3 \times 10^{-5}$ K^{-1}, and $\kappa = 10^{-6}$ m^2 s^{-1}. If the mantle lithosphere varies in temperature between $T_s = 800$ K at the Moho and $T_m = 1600$ K at its base, the temperature variation across the potentially unstable mantle lithosphere is $T_0 = T_m - T_s = 800$ K.

The rheology of mantle lithosphere is thought to be characterized by diffusion

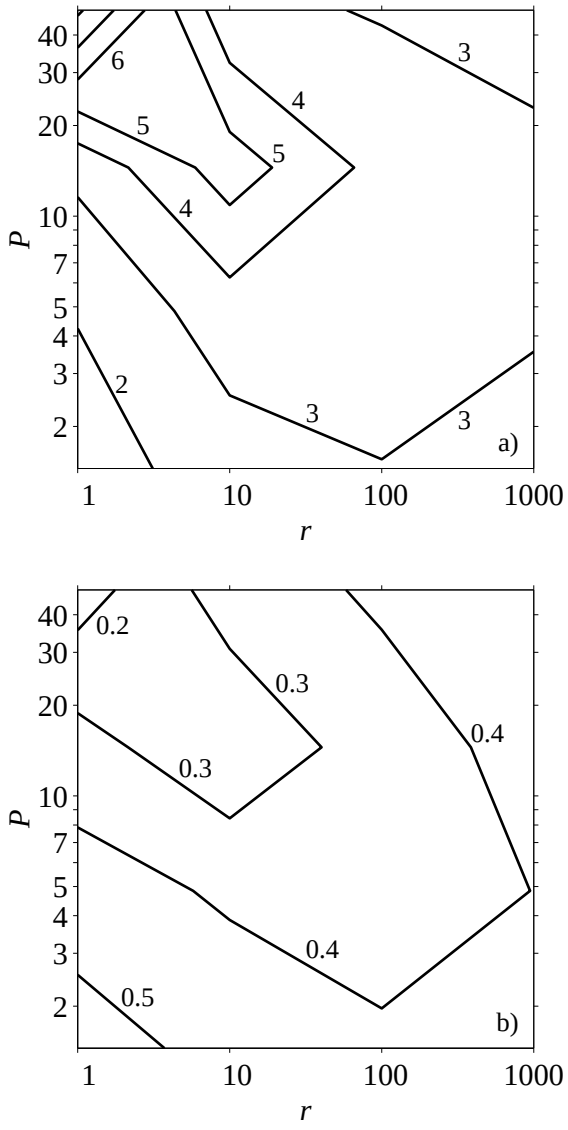

Figure 3.13: Similar to Figure 3.12, but showing measurements taken at t_{100}, the time for 100% thickening (or 50% horizontal shortening) to occur. In this case, both the (a) depth of penetration of the persistent downwelling (given in units of the initial layer thickness) and the (b) temperature of material protruding deeper than the original depth of the $T' = 0.9$ isotherm depend only weakly on both the shortening rate given by P and the temperature-dependence of viscosity given by r.

creep, for which $n = 1$, at stresses lower that 0.1 to 1 MPa, and by dislocation creep, for which $n = 3$ to 3.5, at higher stresses [*Karato, Paterson, and FitzGerald*, 1986]. Convective instability should be accompanied by stresses greater than this, favoring dislocation creep. *Hirth and Kohlstedt* [1996] propose that the mantle is "wet" below 60 to 70 km depth, for which *Karato, Paterson, and FitzGerald* [1986] deduced a power law exponent of $n = 3$, an activation energy of $Q = 420$ kJ/mol, and a preexponential factor of $A = 1.9 \times 10^{-15}$ Pa s^{-3} for olivine. Using these parameter values, *Conrad and Molnar* [1999] estimate $B_m = 1.9 \times 10^9$ Pa s$^{1/3}$. *Hirth and Kohlstedt* [1996], however, assign a power law exponent of $n = 3.5$ to wet olivine. As a result, considerable uncertainty is associated with *Conrad and Molnar's* [1999] estimate of B_m, which is accommodated here by using $n = 3$ and allowing B_m to vary.

The "available buoyancy" parameter F_n accounts for the temperature dependence of B for a given temperature profile in a layer. *Conrad and Molnar* [1999] estimate its value for wet dislocation creep by assuming an activation energy of $Q = 420$ kJ/mol. They find $F_3 = 1.3 \times 10^{-4}$ for an error function temperature profile. If the strain-rates associated with horizontal shortening control the effective viscosity of the layer, this viscosity is constant with perturbation amplitude, meaning that the power law exponent $n = 1$ is applicable. Following *Conrad and Molnar* [1999], $F_1 = 5.7 \times 10^{-2}$ for the error function temperature profile, which is slightly larger than that estimated by *Conrad and Molnar* [1999] for $n = 1$, because their study uses parameters for diffusion creep without horizontal shortening. If the temperature profile is not that of an error function, estimates of the "available buoyancy" should be different from those assumed here. This uncertainty is acceptable, however, because it can be absorbed by the uncertainty associated with the strength parameter B_m.

As described above, the values of Ra_1, Ra_3, and P can be used to determine which of the above-described mechanisms should dominate lithospheric deformation. In particular, their "critical" values (Table 3.1) delineate transitions between different styles of thickening and growth. By plotting the location of these transitions as a function of parameters that can vary, a "phase diagram" can be constructed that shows the dominant style of growth in different regions of the space defined by the

variable parameters. An example diagram (Figure 3.14) shows the typical location of boundaries between the four deformation styles, or "phases," in the space defined by the strength parameter B_m and the time t_{100}, for 100% thickening to occur, which defines the strain-rate according to (3.29). In this case, if both $Ra_3 < 100$ and $Ra_1 < 100$, the layer is convectively stable, with mechanical thickening (**MT**) dominating if $P > 1$ and thickening by thermal diffusion (**TD**) dominating otherwise. If $Ra_1 > 100$, horizontal shortening still dominates if $Z_0' Ra_1 / P < 0.5$, otherwise perturbations grow exponentially (**EG**) with time for $Ra_1 / Ra_3 > 1$ and super-exponentially (**SEG**) otherwise. The locations of these boundaries relative to dimensional values of B_m and t_{100} depend on the parameters used to calculate Ra_1, Ra_3, and P. As a result, diagrams are constructed by plotting the locations of these "critical" values as functions of B_m and t_{100} for the lithospheric parameters given above, perturbation amplitudes of $Z_0' = 10\%$ (Figure 3.15) and $Z_0' = 50\%$ (Figure 3.16), and layer thicknesses of $h = 25$, 50, 100, and 200 km (parts (a) through (d) in Figures 3.15 and 3.16).

The boundaries between dominating styles of thickening or unstable growth change as the mantle lithosphere thickens, or as perturbations to it grow. By considering how these boundaries move due to changes in h or Z, the evolution of the mantle lithosphere's thermal structure can be examined. Consider mantle lithosphere for which $Z_0' = 10\%$, $B_m = 10^{10}$ Pa $s^{1/3}$, $h = 25$ km, and $t_{100} = 50$ million years. Initially, such a lithosphere grows most rapidly by cooling from above (Figure 3.15a). However, as it thickens, Ra_1 increases, causing the transitional boundary of $P = 1$ to move toward larger values of t_{100}. By the time the lithosphere is 50 km thick (Figure 3.15b), such mantle lithosphere grows most rapidly by horizontal shortening. Alternatively, if the shortening rate increases suddenly due to an acceleration of convergence at the surface, t_{100} should suddenly decrease, causing a transition from thermal diffusion to horizontal shortening as the most rapid mechanism for deformation (Figure 3.15a).

The thickness of the mantle lithosphere should continue to increase, either by cooling from above or by horizontal shortening, until the lithospheric layer becomes convectively unstable. In fact, it can be argued that continental lithosphere is prob-

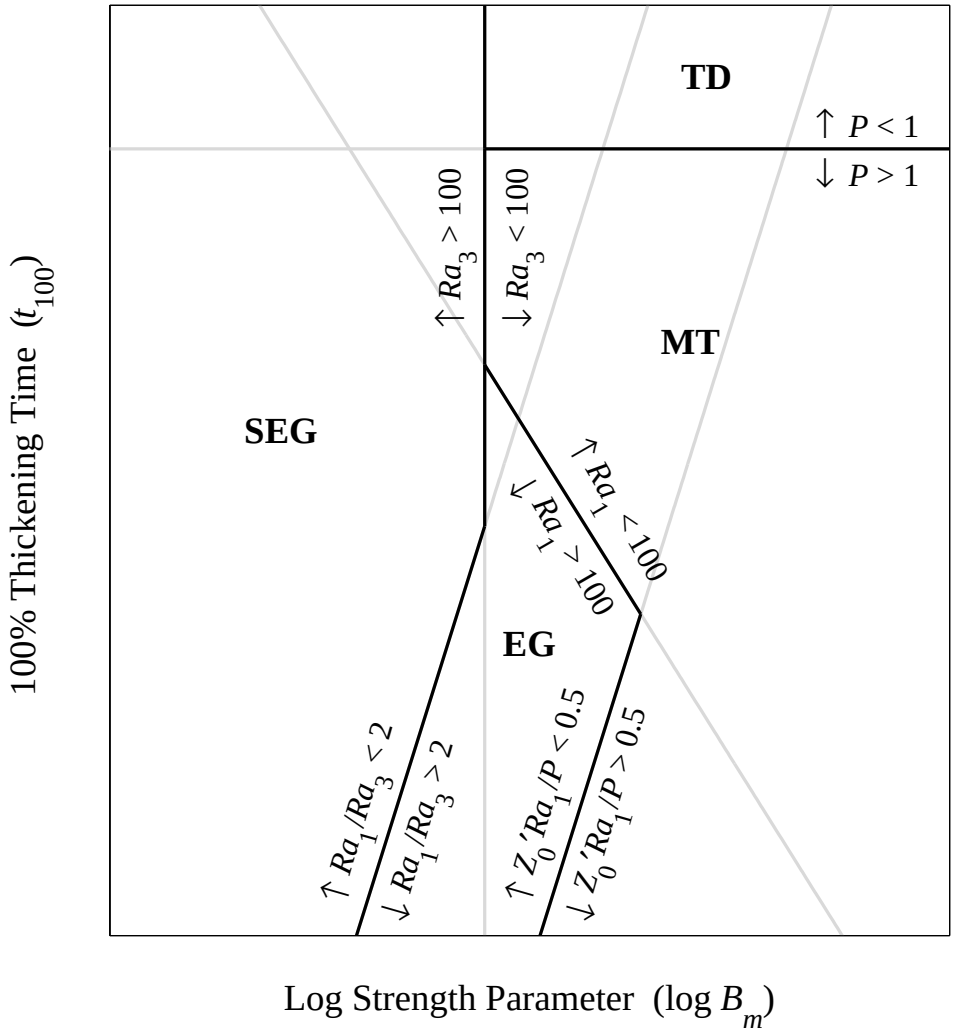

Figure 3.14: A cartoon of a "phase diagram" that shows the dominant style of thickening or growth (the "phases") as a function of the strength parameter B_m and the time, t_{100}, for 100% thickening (or 50% horizontal shortening) to occur. Here, t_{100} defines the background horizontal strain-rate, as in (3.29). The boundaries between each of the four regions are determined by the "critical" values associated with Ra_1, Ra_3, and P, summarized in Table 3.1: $Ra_1 = 100$, $Ra_3 = 100$, $P = 1$, $Ra_1/Ra_3 = 2$, and $Z_0' Ra_1/P = 0.5$. For each line, arrows show the direction in which a quantity increases or decreases away from the line. Light lines show portions of these lines that are not relevant to determining the stability of a given mode. The four mechanisms include: thickening by thermal diffusion (denoted **TD**), mechanical thickening associated with horizontal shortening (denoted **MT**), exponential growth of perturbations (denoted **EG**), and super-exponential growth of perturbations (denoted **SEG**).

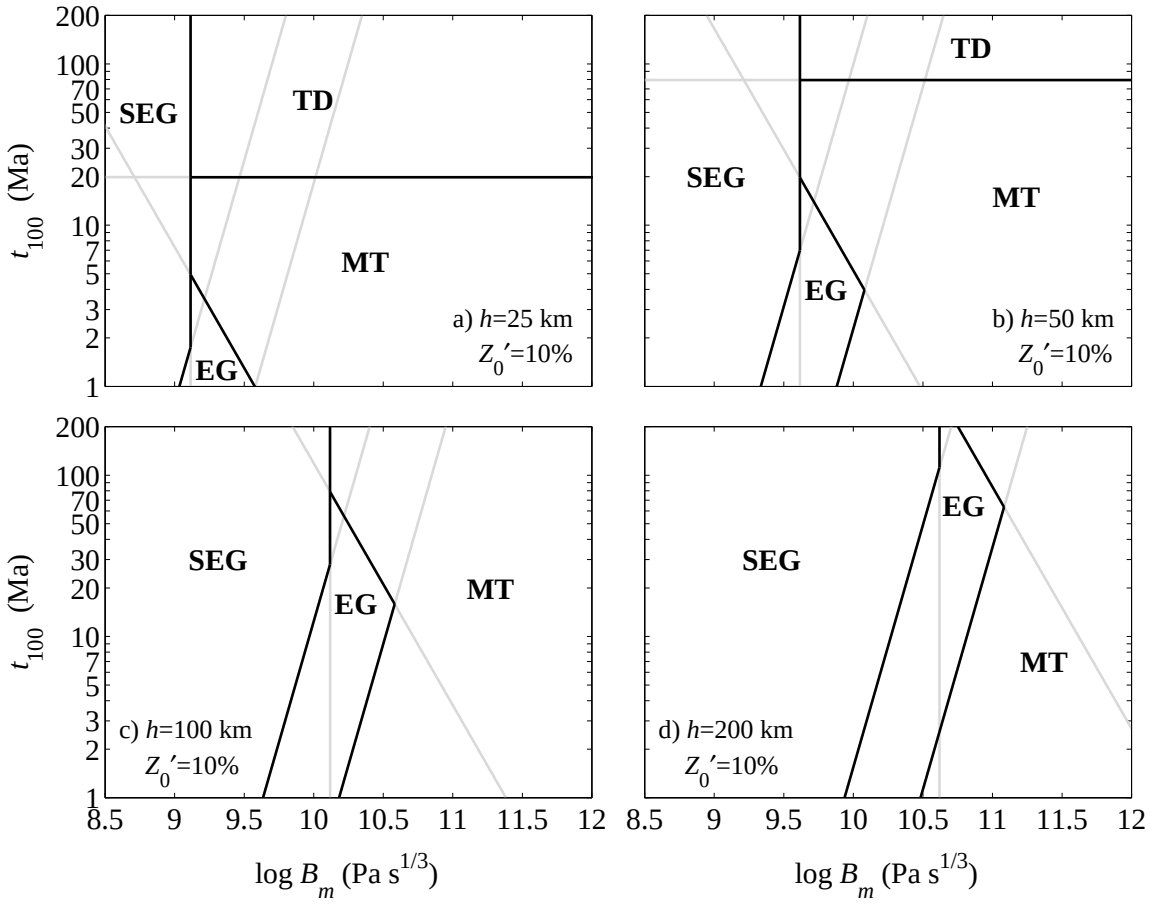

Figure 3.15: "Phase diagrams" similar to the one exemplified in Figure 3.14, but where the parameters relevant to the lithosphere (see text) are used to calculate the locations of boundaries between the different styles of thickening and growth. Shown in (a) through (d) are diagrams for mantle lithosphere with thicknesses of $h = 25$, 50, 100, and 200 km, and for an initial perturbation amplitude of $Z_0' = 10\%$.

ably close to its stability limit for long portions of Earth's history. The lithospheric roots beneath the cratonic shields, for example, are thought to have experienced little deformation since the Archean [e.g., *Hoffman,* 1990]. Without any deformation, cooling from the surface since that time should cause the lithosphere to grow several times thicker than its maximum depth, which has been estimated at up to 200 to 300 km [e.g., *Gaherty and Jordan,* 1995; *Jaupart et al.,* 1998; *Jordan,* 1988; *Simons, Zielhuis, and van der Hilst,* 1999]. Clearly some erosion of the lithospheric base must occur to limit the lithospheric depth, even if the lithospheric root is partially stabilized due

to an inherent chemical buoyancy, as has been proposed for the continental "tectosphere" [e.g., *Jordan*, 1978; 1981; 1988]. If the erosion process involves convective instability, then the continental lithosphere should be at or near its stability limit, which is given by $Ra_1 = 100$ or $Ra_3 = 100$.

Consider mantle lithosphere that is tectonically stable (not shortening) and that has grown to its stability limit, for which $Ra_3 = 100$. The thickness of such lithosphere is given by the value of h that produces $Ra_3 = 100$ for values of Z_0' and B_m appropriate for the lower lithosphere (Figures 3.15 and 3.16). For example, if $Z_0' = 10\%$, and the experimentally observed value of $B_m \sim 10^{9.1}$ Pa $s^{1/3}$ applies, only mantle lithosphere thinner than ~ 25 km is stable to convection (Figure 3.15a). If mantle lithosphere thicker than this value can remain stable, B_m must be greater or Z_0' must be smaller. In fact, an order of magnitude increase in B_m is required to increase the maximum thickness of stable lithosphere to 100 km (Figure 3.15c). An increase in B_m with lithosphere thickness is perhaps expected due to the pressure dependence of dislocation creep [e.g., *Karato and Wu*, 1993]. In addition, it is possible that uncertainties in estimates for F_3, or in the application of laboratory measurements of B_m to the lithosphere, could conspire to permit layers that are more than 100 km thick to be stable to small-scale convection at their base.

If horizontal convergence is applied to a layer that is close to its stability limit ($Ra_3 = 100$), gravitational instability can be initiated rapidly. An increase in the background horizontal strain rate, $\dot{\epsilon}_{xx}$, corresponds to a decrease in the time to 100% thickening, given by t_{100} in (3.29). As shown in Figures 3.15 and 3.16, a sufficiently large decrease in t_{100} along the $Ra_3 = 100$ curve causes exponential growth of perturbations to dominate deformation of the layer. For example, if $B_m \sim 10^{10.1}$ Pa $s^{1/3}$ and $Z_0' = 10\%$, mantle lithosphere of thickness $h = 100$ km is stable to convection if shortening is sufficiently slow that $t_{100} > 80$ Ma (Figure 3.15c). For $t_{100} \sim 30$ million years, as seems to characterize Tibet [*Molnar, England, and Martinod,* 1993], the lithosphere is gravitationally unstable, with perturbations growing exponentially with time (Figure 3.15c). Once perturbations begin to grow, the region for which $Ra_3 > 100$ (super-exponential growth of perturbations) begins to include larger values of B_m (compare

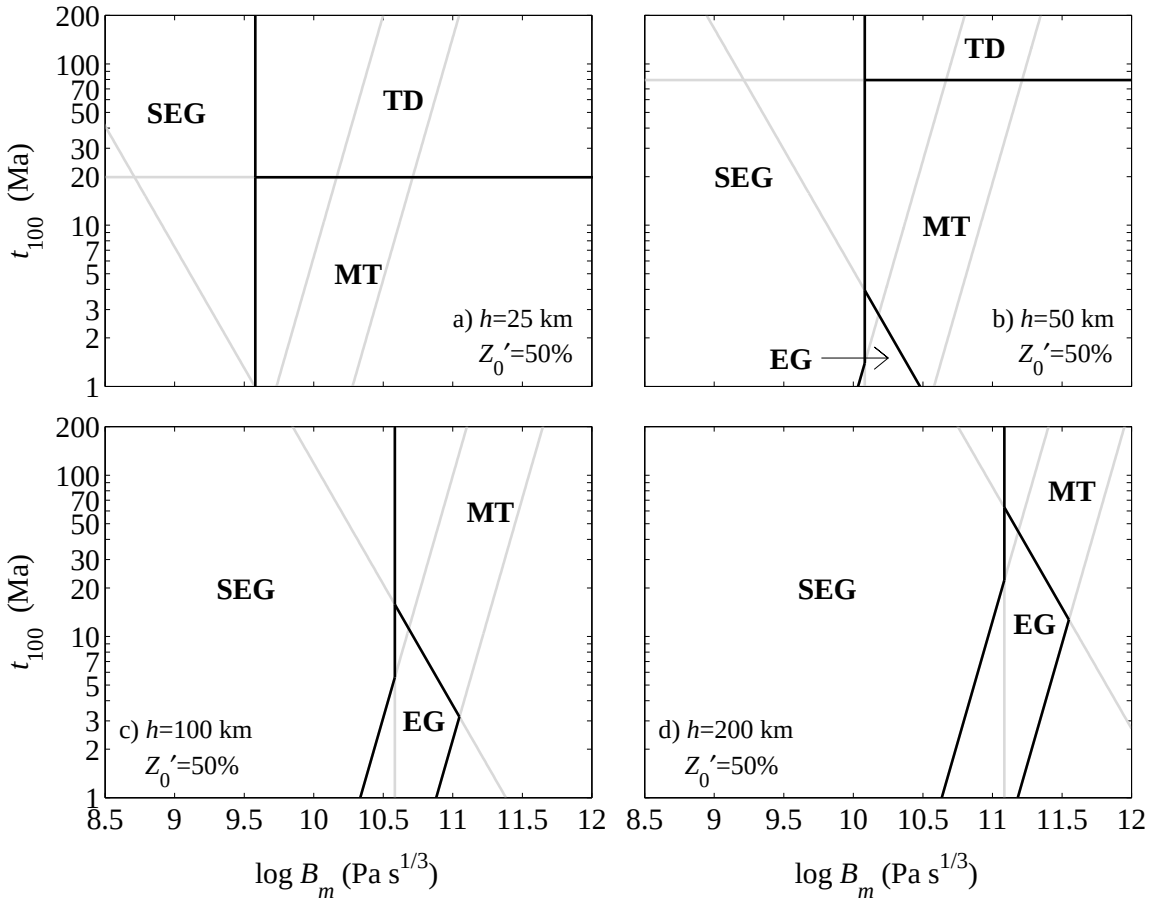

Figure 3.16: Similar to Figure 3.15, but for a perturbation amplitude of $Z_0' = 50\%$. A comparison to Figure 3.15 shows that the region in which super-exponential growth of perturbations dominates (denoted **SEG**) is larger for larger Z_0'.

Figures 3.15 and 3.16). Thus, 100 km thick lithosphere for which $B_m = 10^{10.1}$ Pa s$^{1/3}$ and $t_{100} = 30$ Ma, but for which perturbations have increased to 50%, should exhibit super-exponential growth of perturbations (Figure 3.16c). In fact, if the layer is already at its stability limit before it begins thickening, super-exponential growth should begin after only a small increase in perturbation amplitude, meaning that the majority of the deformation should occur as super-exponential growth.

If the onset of horizontal convergence is not sufficient to initiate exponential growth, super-exponential growth may still develop after sufficient mechanical thickening. First, non-uniform horizontal shortening may increase the amplitude of pertur-

bations, causing the layer to move from a state in which horizontal shortening dominates to one in which super-exponential growth dominates. If $B_m = 10^{10.1}$ Pa $s^{1/3}$ and $h = 100$ km, but t_{100} decreases only to 100 million years, an increase in perturbation amplitudes due to horizontal shortening should still cause super-exponential growth rapidly to become dominant (compare Figures 3.15c and 3.16c). Alternatively, an increase in layer thickness h due to mechanical thickening should cause a marginally stable layer to become unstable (compare the location of $B_m = 10^{10.1}$ Pa $s^{1/3}$ and $t_{100} = 100$ million years in Figures 3.15c and 3.15d).

Once super-exponential growth begins, the time for the initial gravitational instability to remove the bottom part of the mantle lithosphere can be estimated by making t_b' in (3.31) dimensional using (3.5), which for $n = 3$ can be written:

$$t_b = \frac{h^2}{\kappa Ra_3} \frac{1}{2C^3} \tag{3.32}$$

Because super-exponential growth begins when $Ra_3 = 100$, with $C = 0.45$ the removal time can be written as $t_b = 0.055h^2/\kappa$. With $\kappa = 10^{-6}$ m^2 s^{-1}, t_b becomes a function of only the layer thickness, h (Figure 3.17). All of the other parameters that affect growth are eliminated from this expression by the assumption that super-exponential growth begins when $Ra_3 = 100$. If, as discussed above, a phase of exponential growth or shortening precedes super-exponential growth, its duration should be short and thus should not significantly affect this estimate of t_b.

As discussed above, the amount of material removed by the initial instability depends primarily on the temperature-dependence of viscosity. If, as is likely to be the case, viscosity varies by a factor of more than 100 across the mantle lithosphere, at most only the hottest 30% of the mantle portion of the lithosphere is removed (Figure 3.11). If shortening continues after this time, however, the ongoing addition of cold material to the lithosphere is balanced by a persistent downwelling that removes this extra cold mantle lithosphere from the shortening region. If shortening is sufficiently fast and is allowed to occur indefinitely, this downwelling is capable of causing all but the coldest 10% of the mantle lithosphere to be advected into the man-

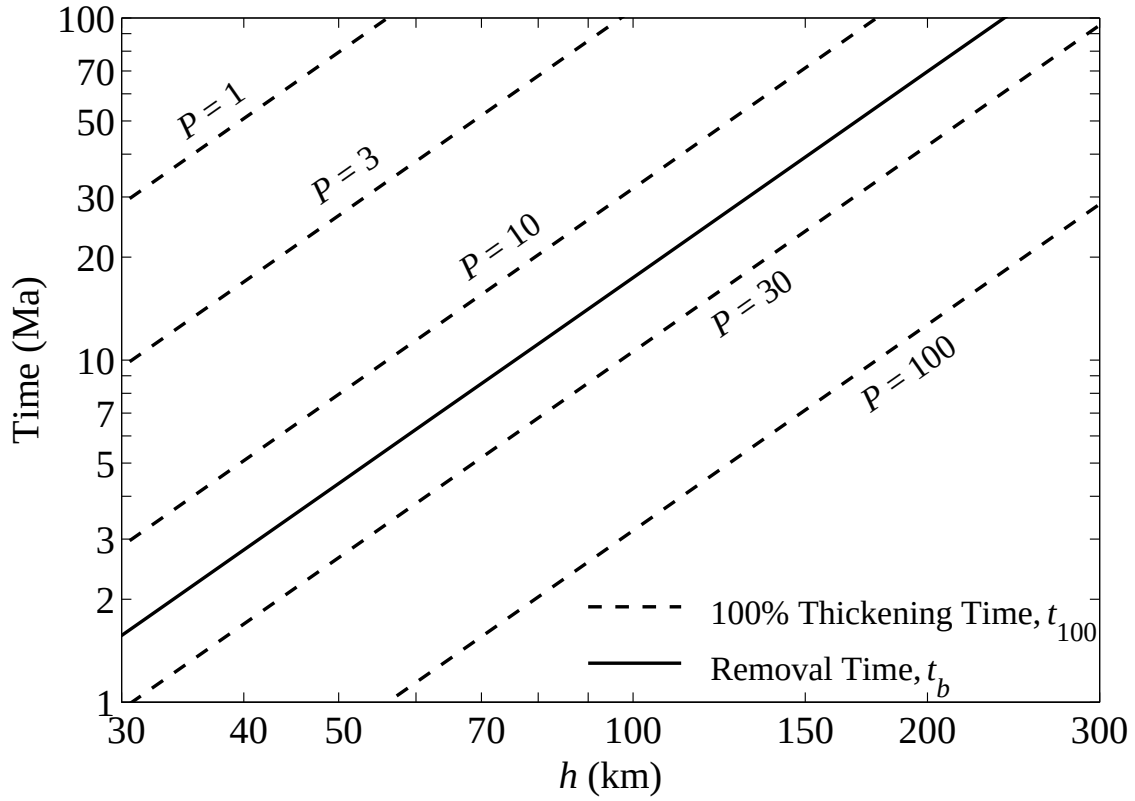

Figure 3.17: Plot of the time, t_b, for the initial instability to remove the base of the mantle lithosphere, and of the time, t_{100}, for 100% thickening of the lithosphere (or 50% horizontal shortening at the surface) to occur. Both t_b and t_{100} are calculated as described in the text as a function of the thickness, h, of the mantle lithosphere. The 100% thickening time depends on the shortening rate, expressed here in terms of P.

tle once shortening stops (Figure 3.12b). Because this persistent downwelling results more from mechanical thickening than from a balance of viscous and gravitational body forces, the amount of material that participates in this downwelling is nearly independent of the temperature-dependence of viscosity (Figure 3.12b).

The total amount of lithospheric shortening that occurs on the Earth may be limited to 50%. As a result, the amount of time during which a persistent downwelling can develop may be limited as well. The time to 50% shortening (100% thickening) can be compared to the time for the initial instability to occur by taking the ratio of t_{100} and t_b using (3.29) and (3.32). Simplifying using $Ra_3 = 100$ and $C = 0.45$ shows that $t_{100} = t_b/(0.055P)$. Thus, the time to 50% shortening is some multiple of the

initial removal time, where this multiple depends on P (Figure 3.17). If shortening is sufficiently fast that $P > 1/0.055 \sim 18$, mechanical thickening of the layer should occur more rapidly than convective instability, meaning that an estimate of t_b is probably not relevant. As shown in Figure 3.17, $P > 18$ requires 100 km thick mantle lithosphere to double in thickness in only 15 million years, and thinner lithosphere to shorten even more rapidly. This is faster than the $\sim$ 30 million years expected for shortening by 50% in Tibet [*Molnar, England, and Martinod,* 1993], but implies horizontal strain-rates of $\sim 10^{-15}\mathrm{s}^{-1}$, which are perhaps not unreasonable for other convergent zones such as the Transverse Ranges of California [e.g., *Houseman et al.,* 1999].

On the other hand, if shortening is slow enough that $P < 18$, then $t_{100} > t_b$, meaning that 50% shortening occurs after the initial removal event. In this case, only the hottest 60% of material is advected into the mantle (Figure 3.13b). Because the persistent downwelling removes material that is advected into the downwelling region, its amplitude depends on the amount of shortening that occurs. Thus, for shortening of 50%, the amount of material that participates in the downwelling is a constant. This amount (the hottest 60%, corresponding to $\sim 500^{\circ}$C of temperature variation if the mantle lithosphere accounts for $\sim 800^{\circ}$C) is a larger fraction of the lithosphere than is observed to participate in the initial instability (at most the hottest 30%, or $\sim 250^{\circ}$C), making the persistent downwelling a potentially more important consequence of shortening than the initial removal event.

A possible limitation of this analysis is that it is performed in only two dimensions, meaning that downwellings necessarily are sheet-like structures. This limitation is perhaps acceptable because this study is designed to treat instability that is generated by horizontal shortening, which, for convergence between two large plates, is inherently a two-dimensional process. Because, however, instabilities grow exponentially or super-exponentially with time, small lateral differences in growth rate can be rapidly amplified, causing a downwelling sheet to have a three-dimensional structure, which could complicate the application of these results to the mantle. In addition, these results treat dislocation creep, for which $n \sim 3$. Thus, regions of low strain-rate

resist flow because their effective viscosity is high. It is possible that flow in the asthenosphere is instead Newtonian, with a viscosity as low as 10^{19} Pa s [e.g., *Hager,* 1991]. In this case, the viscosity beneath the lithosphere would not be dictated by the background shortening rate, and thus would allow the lower lithosphere to be removed more rapidly, even at lower shortening rates than the above analysis suggests. On the other hand, deflection of the Moho is also ignored, which, if driven by convective instability, should tend to resist convective instability because it is gravitationally unfavorable [e.g., *Neil and Houseman,* 1999]. Moho deflection may, however, also promote convective instability by generating large-amplitude perturbations to the mantle lithosphere's thermal structure.

3.8 Conclusions

The theory and numerical experiments described above examine the deformation of unstable mantle lithosphere that is undergoing active shortening. The thermal structure of mantle lithosphere evolves due to four processes. In the absence of convective instability, mantle lithosphere thickens either by horizontal shortening or by cooling from above. Convective instability manifests itself either by exponential growth of perturbations, which requires lithospheric viscosity to be set by the background shortening rate, or by super-exponential growth of these perturbations, in which case viscosity is set by the strain-rates associated with instability. The conditions under which each type of deformation is dominant can be determined by comparing the amplitudes of the dimensionless parameters Ra_1, Ra_3, P, and Z_0', which are defined for this purpose (Table 3.1).

In applying these results, mantle lithosphere is assumed to have cooled sufficiently that $Ra_3 \sim 100$, meaning that it is nearly convectively unstable. In this case, horizontal shortening can easily initiate convective instability by increasing the amplitude of perturbations, either directly through non-uniform thickening, or by lowering the background viscosity so that perturbations begin to grow exponentially with time. Once super-exponential growth begins, the time for removal is approxi-

mately $t_b = 0.055h^2/\kappa$. Thus, for mantle lithosphere 100 km thick, the initial removal event occurs 17 million years after shortening initiates super-exponential growth. For strongly temperature-dependent viscosity, at most only the hottest 30% of the mantle lithosphere is involved in this event.

As shortening of the lithosphere continues, downwelling of lithospheric material persists after the initial removal event. This downwelling removes material that is continually being added to the layer by shortening, and thus is more substantial for larger shortening rates. If, however, the total amount of shortening is limited to 50%, corresponding to thickening of 100% (doubling of crustal thickness), shortening may cease before this downwelling can penetrate into the mantle to its maximum possible depth. Because this persistent downwelling removes material added to the lithosphere by shortening, its amplitude depends on the amount of shortening that occurs. For 50% shortening, the hottest 60% of mantle lithosphere participates in the downwelling, which extends to depths about 3 to 4 times the lithospheric depth. As a result, the downwelling that results from mechanical thickening of the layer is more substantial than the downwelling associated with the initial removal event.

Once mechanical thickening stops after achieving 50% shortening, the persistent downwelling that extends into the mantle beneath the shortening region is no longer replenished by the addition of lithospheric material above it. Because it is a thin feature, as evidenced by the depth (3 to 4 times h) to which only the lower 60% of the mantle lithosphere extends (corresponding to temperatures between about 1100 K and 1600 K), it is not likely to survive once horizontal shortening stops. If this "finger" of cold lithosphere is removed, either due to its own gravitational instability or to mantle shear, its replacement by hot asthenosphere should cause significant uplift at the surface, which could lead to rapid mountain building. The timing of surface uplift should coincide approximately with the end of a period during which 50% shortening is achieved. For Tibet, 50% shortening (doubling of crustal thickness) began at 40 to 50 Ma and is thought to have taken 30 to 40 million years to complete. Rapid uplift at the surface is inferred to begin at approximately 8 Ma [*Harrison et al.,* 1992; *Molnar, England, and Martinod,* 1993], after shortening had ceased within

the interior of Tibet. This pattern is consistent with the gradual building of a cold protrusion into the mantle by horizontal shortening and rapid surface uplift associated with its removal once shortening stops.

Acknowledgments. This work was supported in part by National Science Foundation grant EAR-9725648, and by a National Science Foundation Graduate Research Fellowship. I thank B. Hager for helpful comments and P. Molnar for suggestions and encouragement throughout the preparation of this manuscript that greatly improved its content and clarity.